ISSN 0965-545X, Polymer Science, Series A, 2017, Vol. 59, No. 6, pp. 791–825. © Pleiades Publishing, Ltd., 2017.
Original Russian Text © T.F. Irzhak, V.I. Irzhak, 2017, published in Vysokomolekulyarnye Soedineniya, Seriya A, 2017, Vol. 59, No. 6, pp. 485–522.

REVIEW

Epoxy Nanocomposites

T. F. Irzhak* and V. I. Irzhak

Institute of Problems of Chemical Physics, Russian Academy of Sciences, pr. Akademika Semenova 1, Chernogolovka, Moscow oblast, 142432 Russia

**e-mail: irzhak@icp.ac.ru*

Received February 16, 2017

Abstract—The formation and physical properties of epoxy nanocomposites with carbon (nanotubes, graphene, and graphite), metal-containing, and aluminosilicate (montmorillonite and halloysite) fillers are considered. The mutual effect of both a matrix and nanoparticles on the composite structure is discussed. The role of the interfacial layer in the mechanical properties of nanocomposites is revealed. It is found that the concentration dependence of electrical and thermal conductivities of the composites is related to the percolation phenomenon.

DOI: 10.1134/S0965545X17060049

INTRODUCTION

Since around the mid-1990s, polymer nanocomposites have become the subject of considerable attention, as evidenced by monographs [1–9], including those published in Russian [1–5], and a great quantity of reviews: since 2010 alone, more than two dozen papers have been published [10–34]. The application of nanocomposites is associated with their unique properties related to a huge specific surface and high surface energy of nanoparticles. Nanosized particles, as opposed to microinclusions and coarser inclusions, are not stress concentrators, and this circumstance facilitates a marked improvement in the mechanical properties of nanocomposites. Compared with the respective polymers, the transparency of nanocomposites does not decrease, because nanoparticles do not scatter light because of their small sizes. Depending on the type of nanoparticles introduced in polymeric materials even at a low concentration, nanocomposites acquire remarkable chemical (primarily catalytic), electrophysical, and biomedical properties, thereby opening wide potential for their use.

Among polymer nanocomposites (Fig. 1, curve *1*), it would appear that composites based on an epoxy matrix occupy an unnoticeable place—nearly 10% as to the number of publications—but an ever increasing number of papers appear annually (curve *2*). Moreover, the interest in them grows almost exponentially, as evidenced by the number of citations (curve *3*).

Epoxy polymers in terms of a set of properties stand out among other polymeric materials and play an important role in aerospace, automotive, shipbuilding, and other industries. Their wide application in engineering is associated, firstly, with a high processability of epoxy resins and, secondly, with the unique combination of performance characteristics of their curing products [35–38].

A high reactivity of epoxy groups and a thermodynamic miscibility of epoxy oligomers with many sub-

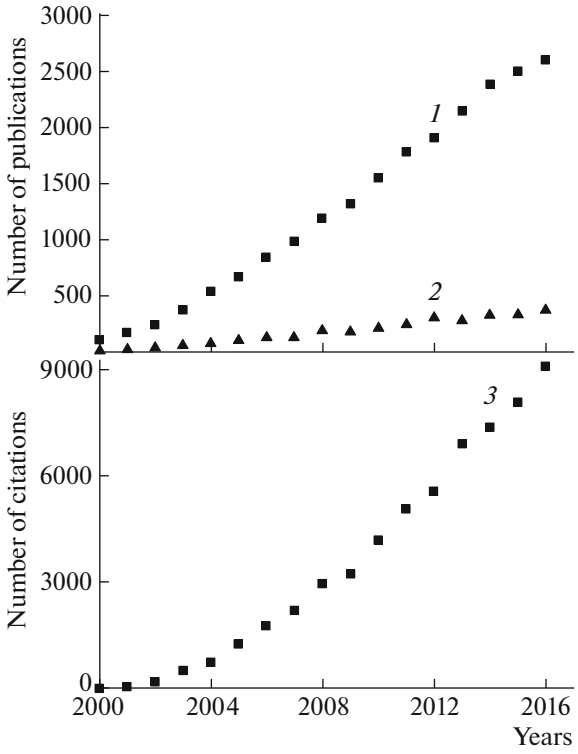

Fig. 1. The number of publications on (*1*) polymeric and (*2*) epoxy nanocomposites and (*3*) the number of their citations according to the Web of Science.

stances make it possible to use diverse curing agents and to accomplish curing reactions under various technological conditions [39–41]. Of no small importance are the features of synthesis processes, such as the absence of volatile products and a low level of shrinkage.

Epoxy polymers have high values of static and shock strength, hardness, and wear resistance. They possess marked thermal stability and heat resistance. Many solid surfaces form strong adhesive bonds with epoxy polymers [35, 36]. This circumstance determines their use as compounds, glues, paint and lacquer materials, and coatings. A special place is occupied by composite materials, including fibrous materials [42], primarily highly filled reinforced plastics, in which high-modulus and high-strength fibers function as load-bearing elements [43]. A matrix is mostly designed to realize the properties of composites in the engineering material. It ensures integrity of the material and the transfer and distribution of inner stresses. Epoxy polymers meet these criteria to a full extent.

Evidently, epoxy nanocomposites are designed to realize to the same extent the unique functional properties of nanoparticles: electric, magnetic, optical, chemical, and biological.

Certain information about epoxy nanocomposites is contained in the above-listed literature sources. Reviews [19, 22] are devoted to epoxy nanocomposites with carbon nanotubes (CNTs). Some aspects of epoxy nanocomposites containing graphene were covered in [16]. Other generalizing papers are unavailable in this field.

Taking into consideration the urgency of the issue and the presence of recent studies not covered in the mentioned reviews, we took a chance to address epoxy nanocomposites containing metal and mineral nanoparticles, graphene, and CNTs and to discuss the processes of their formation and properties.

SYNTHESIS OF EPOXY NANOCOMPOSITES

From the standpoint of formation of epoxy nanocomposites, there are two types of fillers: fillers belonging to the first type are chemically unchanged and should be reduced to the desired size in one way or another. An example is provided by CNTs, diverse minerals, and graphene. Compounds whose chemical nature changes during composite formation belong to the second type. These are, in particular, metal salts, in which cations should be reduced to the zero-valence state.

In contrast to linear polymers, epoxy nanocomposites are obtained only via the curing of epoxy oligomers in the presence of a filler or the corresponding precursor. It is evident that these additives may affect the kinetics of the process and the properties of the resulting matrix. The mechanism of curing of epoxy resins is fairly complicated, because many reactions occur simultaneously and depend on such phenomena as gelation and glass transition [39, 40]. After incorporation of nanoparticles into the epoxy resin, the process of its curing becomes even more complicated. A considerable number of papers concern the kinetics of curing of epoxy systems with various types of nanoparticles.

Kinetics is often analyzed using empirical Eq. (1)

$$\frac{d\alpha}{dt} = (k_1 + k_2\alpha^m)(1-\alpha)^n, \quad (1)$$

$$\frac{d\alpha}{dt} = (k_1 + k_2\alpha)(1-\alpha)^n, \quad (1a)$$

where α is the degree of conversion of epoxy groups; the sum of exponents $m + n$ defines the overall reaction order, which is usually two. Sometimes it is assumed that $m = 1$ (Eq. (1a)). Constants k_1 and k_2 reflect the autocatalytic character of the process.

Carbon Fillers: CNTs, Graphene, Graphite, and Carbon Fiber

Taking into consideration the molecular structure of carbon nanoparticles, in particular, graphene and CNTs [30, 44–48], it may be stated that their influence on the kinetics of the process of curing of epoxy oligomers will be similar. Indeed, graphene, CNTs, and other compounds with the sp^2-hybridized carbon can catalyze diverse organic reactions [49–51]. Their surface energy is fairly high; therefore, the adsorption of various molecules is typical of them [52–55]. The components of epoxy binders are not exceptional in this respect. Adsorbed molecules may be involved in the process of matrix formation in a certain manner.

H. Xie et al. [56] investigated the high-temperature isothermal curing of tetraglycidyl-4,4'-diaminodiphenylmethane with 4,4'-diaminodiphenyl sulfone (DDS) in the presence of multiwall CNTs.

The typical technique used to prepare the reaction mixture for kinetic studies of the process will be described below, and the techniques described in other papers may differ from the typical one only in details.

A mixture of an epoxy resin with preliminarily purified multiwall CNTs was sonificated for 2 h and placed in an oil bath at a temperature of 120°C, and the stoichiometric amount of a curing agent was slowly added under continuous mechanical stirring until formation of a homogeneous mixture. This process took nearly 10 min.

The kinetics was analyzed using Eq. (1). It was found that, with an increase in the concentration of CNTs, constant k_1, which defines the initial rate of reaction, grows, while the corresponding activation energy drops. The autocatalytic constant k_2 is practically unaffected by the presence of tubes. The authors of [56] believe that these effects may be attributed to

the catalytic effect of surface hydroxyl groups that arise as a result of oxidation during the purification of CNTs.

The initial acceleration of the reaction under the action of single-wall CNTs was also observed in [57], but the magnitude of this effect was insignificant. At the same time, the glass-transition temperature T_g decreased, thus suggesting a reduction in the degree of crosslinking of the matrix [39].

E. Esmizadeh et al. [58] studied the effect of concentration and type of CNTs (single-, double-, and multiwall) on the kinetics of reaction between a low-viscosity mixture of epoxy oligomers and amine curing agents. Analysis was conducted in terms of the equation

$$\frac{d\alpha}{dt} = k(T)\alpha^m(1-\alpha)^n. \quad (2)$$

It was shown that the type of CNTs exerts almost no effect on kinetic parameters possibly because of their low concentration (0.01%). At a concentration of 0.1, 0.2, and 0.5%, the rate constant changes nonmonotonically, but on the whole it is lower than that in the absence of CNTs. The energy of activation increases by almost one and a half times (from ~6 to ~9 kJ/mol). The heat of reaction decreases, indicating the incompletion of the process. This is also evidenced by a decrease in the high-elasticity modulus, i.e., matrix network density. In accordance with the authors, the observed effects may be explained by increase in the viscosity and thermal conductivity of the system in the presence of CNTs, although these properties were not estimated.

As was shown by A. Visco et al. [59], multiwall CNTs, when taken at low concentrations (0.5%), slightly accelerate the reaction of amine curing of bisphenol F diglycidyl ether, while at higher concentrations (1.5%) they decelerate this reaction. In the authors' opinion, the rate of the process is affected by a gain in the viscosity of the system.

In [60], the curing of an epoxy resin is regarded as a heterogeneous phase formation process and the role of multiwall CNTs is discussed from this viewpoint. The authors believe that the tubes restrict the local free volume and assist in development of the heterogeneous morphology in a resin, especially at a high content of multiwall CNTs. At the same time, with an increase in their concentration (to 1%), the ultimate heat of reaction increases, while the energy of activation decreases.

The main quantity of kinetic studies is aimed at gaining insight into the effect of functionalized CNTs using DSC. In this case, the data are analyzed as a rule in terms of the generalized formula

$$\frac{d\alpha}{dt} = k(T)f(\alpha). \quad (3)$$

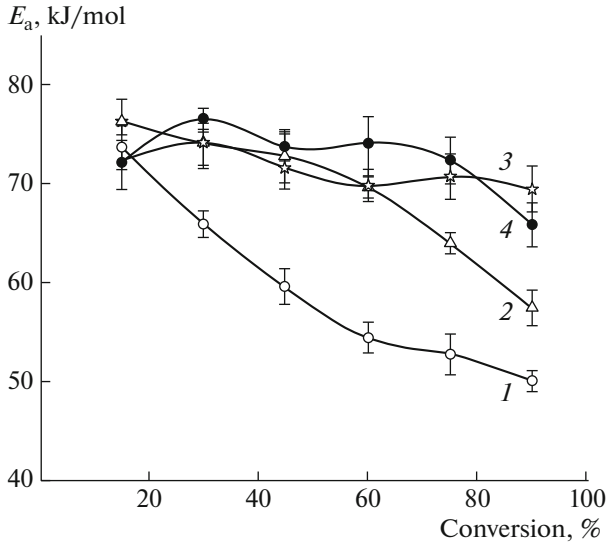

Fig. 2. Dependence of the activation energy on conversion. The concentrations of multiwall CNTs are (*1*) 0, (*2*) 0.1, (*3*) 0.5, and (*4*) 1.0%. The data are taken from [61].

The energy of activation E_a was determined by varying the rate of scanning. Naturally, the value of E_a depended on conversion α.

As an example, Fig. 2 presents the data of A. Rahaman and A. Mohanty [61], who studied the influence of multiwall CNTs carrying COOH groups on the process of curing of epoxy resin EPOLAM with anhydride of 1,2,3,6-tetrahydroxymethyl-1,3,6-methanephthalic acid. According to these authors, this dependence provides evidence that in the presence of multiwall CNTs the degree of crosslinking increases; as a result, the mobility of unreacted groups declines.

Note that methods using the dependence of a change in the exothermal peak on the rate of heating cannot provide reasonable isothermal predictions for the kinetics of curing of epoxy compounds because of the autocatalytic character of the process [39, 40]. The presence of at least two kinetic constants, as in Eq. (1), should be taken into account. An adequate analysis of the situation is available in [62].

In this context, noteworthy are other methods that may be used to advantage depending on the type of investigation or the nature of epoxy resins [63]. Among them, for example, the method of luminescence spectroscopy makes it possible to determine the degree of conversion with a high accuracy at the final stage of reaction. This is hardly achievable in the case of other methods. Analysis with the aid of a rheometer provides information about the time of gelation which cannot be obtained by another method.

The DSC studies of T. Zhou et al. [64] showed that multiwall CNTs act as catalysts, with COOH functionalization stimulating the initial stage of the curing of bisphenol A diglycidyl ether (BADGE). This accel-

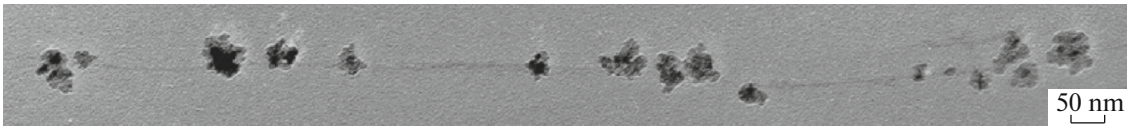

Fig. 3. Initial stage of curing of the epoxy matrix in the presence of COOH-functionalized CNTs. The data are taken from [71].

erating effect is noticeable even at a 1% content of multiwall CNTs. Nonfunctionalized multiwall CNTs decrease the degree of crosslinking, as evidenced by a lower overall heat of reaction and lower glass-transition temperatures of the nanocomposites compared with the neat epoxy resin. At the same time, the functionalization of multiwall CNTs increases the degree of crosslinking.

Compared with the neat epoxy resin, 1% of carboxylated multiwall CNTs decreases the heat of reaction and increases the energy of activation [65]. Fluorinated tubes insignificantly influence the value of E_a but lower the ultimate degree of conversion.

In accordance with L. Valentini et al. [66], the grafting of butylamine onto plasma- and CF_4-treated single-wall CNTs markedly improves the ultimate conversion, whereas neat tubes, when the reaction is accomplished in the nonisothermal regime, have no effect on this parameter, while in the case of the isothermal regime (30°C), they decrease it.

J. Qiu and S. Wang [67] arrived at another conclusion: neat and aminated single-wall CNTs reduce the ultimate heat of reaction. Tubes with the grafted epoxy groups give almost the same value of heat as that obtained in the curing of resin without any filler: 355 versus 362 J/g. It is possible that different results may be attributed to different concentrations of single-wall CNTs. In [66], this value was 0.1%, while in [67] the concentration is not indicated; it appears that this value is much higher.

The kinetic analysis of the curing process in terms of Eq. (1) does not reveal marked differences in the values of constants and exponents for the systems of interest.

However, as was shown in [68], the introduction of 3% of neat multiwall CNTs does not influence the kinetics of reaction, but tubes with grafted amino groups decrease constant k_1 by a factor of almost 2.5, increase k_2 by a factor of 3, and decrease exponent m from 0.53 to 0.27.

K. Yang et al. [69] demonstrated that multiwall CNTs with amino groups decelerate the curing of BADGE with 2-ethyl-4-methylimidazole at concentrations of 0.5 and 1 wt %, but the deceleration effect vanishes at a concentration of nanoparticles of 3%. However, in this case, the value of ultimate heat decreases as well. Note that neat multiwall CNTs accelerate curing of the same reaction system [64].

The impact of multiwall CNTs carrying acidic and amino groups on the process of curing was studied by Raman and luminescence spectroscopy [70]. Throughout the reaction conducted in the presence of nanoparticles, the rates were higher compared with the neat resin. The difference in the rates of curing was explained by homogeneity of the sample and the presence of chemical groups.

S.V. Kondrashev et al. [71] analyzed the kinetics of the amine curing of BADGE in the presence of multiwall CNTs functionalized by oxygen-containing groups using viscometry and transmission electron microscopy along with calorimetry.

The samples of multiwall CNTs had different values of specific surface S. This factor was found to be decisive in the kinetic study of reaction: if at the onset the rates were equal, then, by the time of attaining the maximum rate W_{max}, the higher the value of S, the more pronounced the deceleration of the process, so that the time of attaining W_{max} increased. Afterwards, the inverse effect was observed, namely, acceleration, so that the higher the value of S, the more pronounced the final heat release. The rheokinetic study demonstrated that the time of a sharp gain in viscosity of the system (the gel point) also shifts to longer times with an increase in S. However, variation in the concentration of multiwall CNTs (to 5%) insignificantly influences the kinetics of reaction.

The kinetic features of the process may become understandable if the micrograph of the epoxy composition which is measured at the initial stage of curing performed in the presence of multiwall CNTs is examined (Fig. 3). It is seen that compact polymer structures grow along the tube. Evidently, hydroxyl groups grafted on the surface catalyze the reaction of epoxy groups with amine [40] to give rise to new hydroxyl groups accelerating this reaction. In doing so, the process of polymer formation is localized and the reaction assumes the frontal character. The natural consequence of the localization process is the formation of ineffective crosslinks. Therefore, the value of critical conversion increases and correlation is observed between the time of a sharp gain in viscosity and the specific surface of multiwall CNTs.

As was shown in [72], graphene oxide (GO) accelerates the curing of tetraglycidyl-4,4'-diaminodiphenylmethane with 4,4'-diaminodiphenyl sulfone. According to [72], this effect is related to the presence of hydroxyl and carboxyl groups on the surface of GO.

S.H. Ryu et al. [73] investigated the kinetics of the nonisothermal curing of BADGE with liquid poly(amido amine) in the presence of amine-functionalized GO using Eq. (2). It is seen that, for the systems without any filler and in the presence of GO containing NH_2 groups, the parameters of this equation are similar. At the same time, GO slightly decelerates the process.

J.K. Park and D.S. Kim [74] cured a mixture of BADGE and 1,1,2,2-tetra(*p*-hydroxyphenyl)ethane tetraglycidyl ether with diethyltoluenediamine in the presence of graphene and showed that the latter somewhat accelerates the reaction and increases T_g by 15–25°C. Previously, the same authors showed using Eq. (1) that this effect is associated with an increase in constant k_1 and the functionalization of graphene by amine enhances the effect of the filler [75].

The IR spectral analysis of the curing of BADGE with 4,4'-diaminodiphenylmethane in the presence of GO allowed D.G.D. Galpaya et al. [76] to obtain kinetic curves for both epoxy groups and primary, secondary, and tertiary amino groups. These studies made a considerable contribution to gaining insight into the mechanism of reaction. It was shown that the original GO has no effect on the overall kinetics of the process and even decelerates the consumption of primary amino groups. But after autoclave purification, GO increases the rate of reaction of epoxy groups by more than a factor of 2 and the rate of reaction of primary amino groups by a factor of 1.8. As was shown by X-ray photoelectron spectroscopy, purification leads to a marked reduction in the amount of oxygen-containing groups on the surface of GO.

The glass-transition temperature of a nanocomposite based on the crude GO is much lower than that of the epoxy matrix, whereas the purification of GO causes an increase in this parameter, although T_g does not attain the T_g value of the matrix.

The authors of [77] studied the influence of various graphite fillers (graphite with a high surface area, graphite oxide, and exfoliated graphite oxide) on the reaction of epoxy ring opening of BADGE by amines—primary (benzylamine and cyclohexylamine) and secondary (dibenzylamine)—and hydroxyl (benzyl alcohol). These data indicate a strong catalytic effect of fillers on the reaction with amines. This effect is the most pronounced for the exfoliated graphite oxide. In the case of benzyl alcohol, interaction with epoxy groups was observed only for graphite oxide.

A similar effect was exerted by fillers on the process of matrix formation: in the presence of graphite fillers, the rate and heat effect of the reaction grow and the gel point shifts to smaller times.

In essence, analogous data were reported by M. Mauro et al. [78]. These authors believe that a marked rise in the T_g of nanocomposites compared with the neat matrix is evidence for the catalytic effect of graphite with a high surface area (308 m^2/g) and graphite oxide. The catalytic effect of graphites was confirmed using the reaction of epoxystyrene with benzylamine.

On the other hand, L. Li et al. [79] found that the samples of graphite oxide with carboxyl or amino groups have almost no effect on the kinetics of the nonisothermal curing of BADGE with 4,4'-diaminodiphenylmethane. Possibly, this is related to a low concentration of the fillers (0.5%).

In [80], the effect of carbon nanofibers (a diameter of 100–200 nm and a length of 30–100 μm) oxidized in a solution of nitric acid and then treated with 3-glycidoxypropyltrimethoxysilane on the kinetics of curing of epoxy resin Cycom 977 described by Eq. (1) was studied. It was shown that all kinds of fibers exert a catalytic effect which manifests itself as an increase in ultimate conversion and growth of kinetic constants k_1 and k_2. Note that E_{a1} decreases, while E_{a2} increases. In terms of catalytic efficiency the fibers may be arranged in the following sequence: untreated, oxidized (COOH groups on the surface), and treated with silane (epoxy groups on the surface).

The catalytic effect of a carbon nanofiber was observed in [81]: the ultimate conversion and the kinetic constants in Eq. (1) increase, while the respective activation energies decrease. An even higher activity is exhibited by a fiber whose surface is modified through the oxidative polymerization of aniline (in accordance with the authors, the "nanograssy" coating).

The above results are fairly contradictory. Most likely, this circumstance may be explained by ambiguity with respect to the filler concentration and uncertainty in the degree of dispersion and in the value and structure of its surface.

Noncarbon Fillers: Oxides of Metals and Silicon

R. Sanctuary et al. [82] explored the effect of Al_2O_3 nanoparticles on the kinetics of polycondensation of BADGE under the action of diethylenetriamine using modulated DSC. As a result, not only the rate of the process was registered, but also variation in the heat capacity of the system during the process was monitored. It was shown that the filler increases the rate of reaction but decreases the ultimate heat. Viscosity measurements confirmed that the formation of the polymer network accelerates in the presence of nanoparticles and the gel point shifts not only with time but also with conversion. This implies that nanoparticles are directly involved in the formation of intermolecular bonds. At the same time, experiments with water additives [83] revealed that nanoparticles affect the kinetics of the curing reaction in qualitatively the same manner as Al_2O_3 nanoparticles. The

authors of [83] inferred that water adsorbed by nanoparticles is responsible for the catalytic effect.

The authors of [84] used DSC to examine the effect of additives of Al_2O_3 and ZnO nanoparticles on the curing of BADGE with *o*-tolylbiguanidine. Both oxides decelerate the reaction but increase the ultimate limiting degree of conversion. Exponents *m* and *n* in Eq. (2) remain almost unchanged, whereas the activation energy decreases. Note that in the case of ZnO this decrease is considerable.

In accordance with [85], at a fairly low concentration (1 and 5%), ZnO nanoparticles accelerate the reaction of BADGE with 2,2'-diamino-1,1'-binaphthyl; at a concentration of 10%, their catalytic efficiency declines, while at a content of 15% retardation is observed. Compared with the neat matrix, nanocomposites feature higher values of ultimate heat and glass-transition temperature with the maximum values corresponding to the 5% content of nanoparticles. Probably, reduction in the catalytic activity of nanoparticles with increasing concentration may be attributed to their aggregation; as a result, the effective surface decreases.

M. Ghaffari et al. studied how the size of ZnO nanoparticles affects the kinetics of BADGE curing with poly(amino amide) [86]. Nanoparticles were sheets with a thickness of nearly 20–40 nm, while microparticles were rods with a length of ~1 μm. Analysis was performed using Eq. (2). It was found that the autocatalysis of reaction is absent; that is, $m = 0$ and *n* is somewhat above unity. For both composites, compared with the neat matrix, the energy of activation decreases, but the rate constant slightly grows in the case of the microcomposite and declines in the case of the nanocomposite.

O. Zabihi et al. [87] cured BADGE with the propylenimine dendrimer carrying eight end groups $-NH_2$ in the presence of Fe_2O_3 nanoparticles. The latter manifested the catalytic effect. The higher the concentration nanoparticles, the more pronounced the increase in ultimate conversion and glass-transition temperature. It is shown that the kinetics of formation of a nanocomposite containing 10% Fe_2O_3 is adequately described by Eq. (1a). As regards other systems, including the neat matrix, no data are available. A similar result was reported by the authors of [88], who showed that the kinetics of curing of glycerol diglycidyl ether with 3,3'-dimethylglutaric anhydride in the presence of Al_2O_3 obeys Eq. (1a).

Nanoparticles of metal oxides are able to adsorb components of the reaction system to one extent or another [89]. Possibly, their kinetic role is associated with this property.

Direct measurements of the complex specific heat capacity [90] demonstrated that the interaction of SiO_2 nanoparticles and BADGE molecules is very weak. At all stages of polymer network formation, the interaction of nanoparticles and matrix is of a physical origin. The effect of the filler on the kinetics of curing was insignificant.

In contrast, acceleration of the process was observed in [91, 92]. The kinetic studies [93] revealed that the catalytic effect of SiO_2 nanoparticles is related to the presence of hydroxyl groups on their surface. When the latter groups are changed for epoxy groups, the effect of nanoparticles on the kinetics of BADGE reaction with *m*-phenylenediamine is eliminated.

Minerals

For polymer nanocomposites, the most popular fillers from the class of minerals are layered silicates [94], which are sometimes called nanoclays, in particular, montmorillonite (MMT). The structure of its crystal lattice is such that it can adsorb various ions (mostly cations) and swell in polar liquids owing to their penetration into the interlayer space [95, 96].

At the nanometer scale, MMT is composed of three-layer stacks ~0.7 nm in thickness and several hundred nanometers in length and width. At the micron level, these stacks are united into primary particles with an interlayer distance of about 1.35 nm. At a higher level, they form aggregates. During formation of nanocomposites, stacks should be exfoliated in order to reach a high area of contact with the matrix. In order to facilitate exfoliation, the surface of stacks should be treated for the purpose of changing their hydrophilic nature to hydrophobic, because the hydrophilic character of the silicate surface hampers the dispersion of MMT. Neutral organic compounds may form complexes with interlayer cations; for example, alkylamines are transformed into alkylammonium cations.

These properties of MMT govern the kinetic features of formation of epoxy nanocomposites.

In the absence of the curing agent (1,3-phenylenediamine), the modified MMT and even the unmodified MMT promotes the homopolymerization of BADGE at a high temperature [97]. Depending on the nature of the intercalated modifier (octadecyl-, trimethylstearyl-, methyldihydroxyethylammonium), MMT may either catalyze the reaction of the epoxy oligomer or react with a prepolymer or a curing agent.

At the same time, it was found that MMTs modified with alkylamines weakly accelerate [98–100], retard [101], or do not affect at all [102] the kinetics of curing of epoxy oligomers with amines. A weak acceleration was also observed in [103] for the unmodified MMT and MMT with intercalated 3-aminopropylethoxysilane.

Thus, it should be stated that the rate of curing of epoxy oligomers is almost insensitive to the presence of MMT. However, the kinetics of formation of polymers is not reduced only to a change in the concentration of reactants: structure formation should be taken

into account. Even to a higher extent, this applies to a nanocomposite, whose properties are determined not only by structural levels of the polymer matrix but also by the structure of nanoparticles and the character of their distribution in the material bulk.

As was noted above, MMT needs exfoliation. Exactly this process occurs during the chemical reaction, and its efficiency depends on the reaction conditions. For example, it was shown [104] that the cationic polymerization of triglycidyl-*p*-aminophenol occurs within the interlayer space, which entails the exfoliation of MMT, whereas with DDS the epoxy oligomer reacts outside the interlayer cavity. An increase in temperature is favorable for the former reaction: ultimate conversions inside and outside the cavity are 0.19 and 0.74, respectively, at 120°C or 0.76 and 0.77 at 180°C.

The optimum structure of epoxy composites was achieved when BADGE was cured with poly(ester diamine) in the nonisothermal regime at a low rise in temperature (2.5 and 5 K/min) [105]. Small-angle X-ray scattering studies revealed the exfoliation of MMT in the matrix. The authors of [106] used hyperbranched polyethylenimine with end amino groups as a curing agent and attained effective exfoliation. A comparison of three systems, such as triglycidyl-*p*-aminophenol + DDS, BADGE + poly(ester diamine), and BADGE + hyperbranched polyethylenimine, showed [107] that the exfoliation ability of MMT decreases in the mentioned sequence.

As was reported in [108], the nonisothermal curing of epoxy oligomers with amines in the presence of MMT includes four different reactions: formation of the matrix via the interaction of epoxy groups with the diamine curing agent, intracavity homopolymerization, and two homopolymerization reactions outside MMT which are catalyzed by onium ions of organically modified clay and tertiary amines.

D. Kong and C.E. Park [109] applied X-ray diffraction to probe the exfoliation of MMT intercalated by octadecylammonium during the isothermal curing of BADGE with DDS and showed that this process may be divided into three different stages (Fig. 4).

The first stage is related to the penetration of BADGE into the interlayer space of MMT; at the second stage, the cationic polymerization of the epoxy resin catalyzed by ammonium takes place; and at the third stage, BADGE sorbed by MMT is cured with amine.

In order to identify the intracavity polymerization, a mixture of MMT and triglycidyl-*p*-aminophenol was held at various temperatures for tens of days in the absence of the amine curing agent. Afterwards, DDS was added and the curing process was conducted in the nonisothermal regime [110]. A similar trick was employed for the system BADGE–MMT–poly(ester diamine) [111]. At the first stage, the epoxy equivalent and the glass-transition temperature increased. This

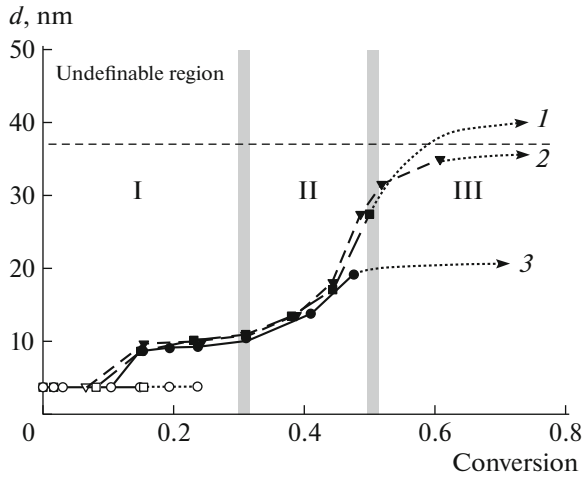

Fig. 4. Change in distance *d* between MMT sheets during the isothermal curing of BADGE at (*1*) 140, (*2*) 130, and (*3*) 120°C. Roman numerals denote stages of the exfoliation process. Arrows indicate the expected tendency of exfoliation. The data are taken from [109].

technology makes it possible to improve both the degree of dispersion of MMT in the epoxy resin and the subsequent exfoliation of the clay during formation of epoxy nanocomposites.

In [112], the period of the intracavity polymerization was reduced to tens of minutes owing to the use of complex $BF_3 \cdot C_2H_5NH_2$ as a catalyst.

S.B. Jagtap et al. [113] made an attempt to accomplish the intracavity polycondensation. As opposed to the commonly used MMT modifiers, i.e., polyalkylamines, they used half neutralized salt of poly(ester diamine), which was intercalated via ionic exchange in an aqueous–organic solution, assuming that these macromolecules, when fixed by the ionic end on the walls of the cavity, will react with epoxy groups of the binder via its free amine end. However, no direct evidence for this reaction is available in [113].

Metal-Containing Nanoparticles Synthesized In Situ

The synthesis of metal-containing nanoparticles meant for producing nanocomposites may be accomplished under the action of various physical processes on the preformed matrix containing molecules of appropriate precursors [3, 4, 114–117]. Physical methods of obtaining metal-containing nanoparticles (photolysis, radiolysis, and thermolysis) are as a rule accompanied by chemical reactions leading to their formation. An important factor is the diffusion of the formed primary substances (metal atoms): the glassy state of the matrix provides a considerable obstacle to diffusion. For example, *N*-cetylpyridinium tetrachloroaurate synthesized in [118] was dissolved in methyl methacrylate and, after polymerization of the latter, was subjected to UV radiation. However, the forma-

tion of gold nanoparticles was registered only at temperatures above T_g of the polymer.

A substantially different method involves the combination of processes of formation of a matrix and metal-containing nanoparticles, i.e., formation of the nanocomposites in situ.

The main chemical method used at moderate temperatures includes the reduction of chemically bound metal atoms in nonpolar media. Exactly chemical reduction methods are the subject of the greatest number of publications [114, 116, 119–125]. Mechanisms controlling formation of metal-containing nanoparticles in situ are highlighted in the review [126].

As precursors soluble in organics, complexes of univalent gold $[O(AuPR_3)_3](CF_3SO_3)$ (R = Ph or CH_3) [127], $[RN(CH_3)_3][Au(SC_{12}H_{25})_2]$ (R = C_8H_{17}, $C_{12}H_{25}$, and $C_{14}H_{29}$), and $[(C_{18}H_{37})_2N(CH_3)_2][Au(SC_{12}H_{25})_2]$ were proposed [128]; salts of organic acids with a fairly bulky (even high-molecular-mass [129–131]) radical, such as silver myristate $C_{13}H_{27}COOAg$, copper oleate $(C_{18}H_{33}COO)_2Cu$, silver oleate, silver octanoate $C_7H_{15}COOAg$, silver stearate $C_{17}H_{35}COOAg$, silver 2-hexyldecanoate p-$C_8H_{17}CH(n$-$C_6H_{13})COOAg$, *cis*-9-octadecanoate p-$C_8H_{17}CH{=}CH(CH_2)_7COOAg$, and silver neodecanoate $CH_3(CH_2)_3C(CH_3)_2COOAg$, have enjoyed popularity [132–140].

However, the nonideal state of solutions of these compounds should be taken into account. This implies that, when a certain value is exceeded, precursors in solution are united into associates, i.e., are clustered. Evidently, this circumstance cannot be disregarded when considering feasible mechanisms governing formation of metal-containing nanoparticles.

L.I. Kuzub et al. [161, 162] synthesized silver nanoparticles by the reduction of alkyl carboxylates in trimethylamine at 78°C. It was found that the induction period grows and the maximum rate decreases in the following sequence: decanoate, myristate, and stearate. But in this sequence, the length of the hydrocarbon radical of carboxylates (C_9, C_{13}, and C_{17}) increases. It is reasonable to assume that solubility grows in the same sequence and, hence, the possibility of formation of clusters decreases. Thus, there is a direct relationship between the rate of formation of nanoparticles and the concentration of precursor clusters.

This idea underlies the theory of formation of metal-containing nanoparticles from precursors of the silver carboxylates type via their reduction which was put forth by M.E. Solov'ev et al. [143].

The model adopted for formation of metal-containing nanoparticles may be presented as follows. Carboxylates reversibly form triangular and tetrahedral clusters. The development of larger clusters is not allowed because of steric reasons. The reduction of cation in them occurs. As a result, the adsorption of new salt molecules becomes possible. Indeed, if for carboxylates the tetrahedral structure is limiting, then the metal atom in the limit may be surrounded by 12 molecules (the icosahedron structure). It is assumed that the concentration of the reducing agent is high, so that the corresponding reaction is pseudo first order. Thus, the kinetic scheme may be written as follows:

$$\begin{gathered} 3R_{01} \xrightarrow{k_1} R_{03} \xrightarrow{k_2} 3R_{01} \\ R_{01} + R_{03} \xrightarrow{k_3} R_{04} \xrightarrow{k_4} R_{01} + R_{03} \\ R_{01} + R_{ji} \xrightarrow{k_3} R_{j,i+1} \\ R_{ji} \xrightarrow{k_4} R_{01} + R_{j,i-1} \\ R_{ji} \xrightarrow{k_5} R_{j+1,i-1} \end{gathered} \qquad (4)$$

(i = 0, 1, 2, ...; j = 3, 4,...). Here R_{ji} denote clusters composed of i carboxylate molecules and j atoms of the zero-valence metal. Accordingly, R_{01} is the initial carboxylate, R_{03} is the cluster of the triangular carboxylate, and R_{04} is the cluster of the tetrahedral carboxylate. Reactions with constants k_1 and k_2 are responsible for the formation and dissociation of associates consisting of three carboxylate molecules, and reactions with constants k_3 and k_4 correspond to the addition of one molecule to cluster R_{ji} and its detachment. The reaction with constant k_5 involves reduction of the bound metal in a cluster.

A system of equations corresponding to scheme (4) was analyzed with a wide variation in kinetic constants. It was shown that the values of k_2, k_4, and k_5 have a slight effect on kinetics of the process. The decisive role is played by constants k_1 and k_3, that is, those constants that determine reactions giving rise to clusters, including mixed clusters.

The kinetics of the process is characterized by existence of the induction period in the reaction of carboxylate consumption and an almost linear growth of average sizes of metal-containing nanoparticles with conversion. With increase in constant k_1, the maximum rate increases, the induction period shortens, and the sizes of resulting particles decrease. At the same time, the narrow size distribution is typical of these particles.

Papers addressing methods of in situ obtainment of epoxy nanocomposites with metal nanoparticles are scarce. Below we will concern studies published during the last decade.

Under UV radiation 2,2'-dimethoxy-2-phenylacetophenone decomposes into radicals. A dimethoxyphenylcarbonium radical reacts with $AgSbF_6$ and reduces a silver cation to Ag(0) via the transfer of electron, and then the radical transforms into the carbonium cation able to initiate the polymerization of diepoxide. Hence, silver nanoparticles and network matrix are formed simultaneously [144]. With increasing concentration of silver salt, the rate of polymerization and the ultimate conversion decrease, but the glass-transition temperature increases.

L. Vescovo et al. [145] varied the concentration of $AgSbF_6$ in a wide range and determined the yield of silver nanoparticles (Fig. 5). In part, these results were proved in [146]. As is seen, an almost full conversion was attained (the amount of Ag is 31% of the precursor mass).

Y. Yagci et al. [147–149] synthesized silver nanoparticles using the same precursor, $AgSbF_6$, but in the presence of 3,5-bis(4-methoxyphenyl)dithieno[3,2-b;2,3d]-thiophene degradable under irradiation with visible light [147]. A similar technique was employed to synthesize epoxy nanocomposites with nanoparticles of silver [148] and gold [149], but 2,3-bornadione (camphorquinone) was used as a source of radicals; in the case of gold, the precursor was $HAuCl_4$.

J. Lu et al. [150] synthesized silver nanoparticles in situ via the reduction of $AgNO_3$ in the epoxy resin by Triton-100, which simultaneously functioned as a stabilizer of nanoparticles. A cycloaliphatic epoxy resin, hexahydro-4-methylphthalic anhydride as a curing agent, a reducing agent, and a precursor were dissolved in acetonitrile and exposed to UV radiation. After completion of the process, the solvent was removed at a reduced pressure.

It is supposed [151] that in this case the role of irradiation is insignificant; it is more probable that reduction occurs via the following mechanism

$$-OH + Ag^+ \rightarrow -COOH + Ag(0),$$

where –OH is the end group of the reducing agent.

In [152], a complex of silver acetate and 2-ethyl-4-methylimidazole was synthesized in an epoxy resin and during its curing Ag^+ was reduced to Ag(0) as a result of thermal decomposition of the complex. In such a manner, silver nanoparticles were generated in situ. The imidazole product of complex decomposition served as a curing agent.

L.M. Bogdanova et al. [153–155] cured the epoxy resin ED-20 with triethylamine in the presence of silver myristate. The reduction of the latter and the formation of silver nanoparticles occurred simultaneously during polymerization. Reduction agents were both amine and the epoxy group. Carboxylate groups compatible with the medium functioned as stabilizers of particles.

The distinctive feature of formation of nanoparticles in the curing epoxy matrix is that this process occurs under conditions of a growing viscosity and eventually glass transition of the system. In principle, this may transfer any stage of the process from the kinetic to diffusion region: nucleation, growth of nanoparticles via addition of zero-valence atoms, and secondary reactions of the coalescence type or Ostwald ripening. Indeed, as was shown in [155], in the isothermal regime at 70°C, the process decelerates because of glass transition. An increase in temperature to 130°C leads to its "reanimation." At a 3% content of triethanolamine, the volume concentration of nanoparticles grows. Compared with the isothermal curing, the number of nanoparticles remains at the same level, but their size grows. However, at a 5% amount of triethanolamine, the volume concentration of nanoparticles does not grow, although their size increases, while their number shows the tendency toward decline; that is, the process of aggregation occurs.

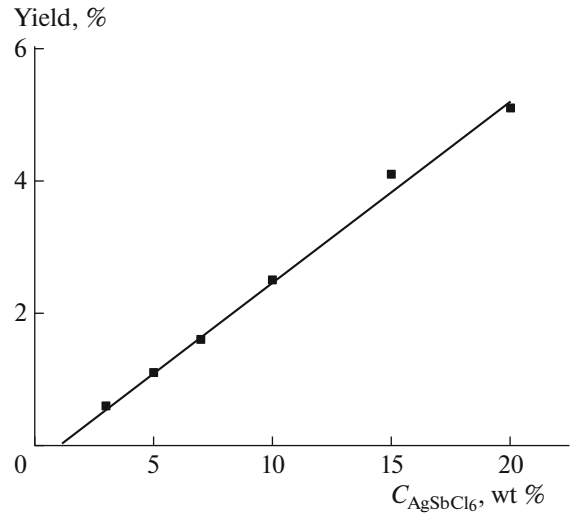

Fig. 5. Dependence of the yield of silver nanoparticles on concentration of the precursor. The data are taken from [146].

STRUCTURE AND PROPERTIES OF EPOXY NANOCOMPOSITES

The properties of polymer nanocomposites are defined by the structure of the matrix, by the type and character of distribution of nanoparticles within the volume, and, finally, by the value and nature of the interfacial layer. In the case of epoxy nanocomposites, these factors are laid to a considerable extent at the stage of synthesis. Many examples are given above as both the matrix and distribution of, say, MMT within the volume. However, the issue regarding formation of the interfacial layer remained uncovered.

Interfacial Layer

As was shown in many papers, mostly using the nanoindentation method ([156–162]), regardless of the nature of fiber and matrix, the interfacial layer extends by micrometers in polymeric fibrous composites. It is evident that the same situation should be expected in the case of nanocomposites.

Indeed, the surface energy of nanoparticles is fairly high; therefore, the adsorption of various molecules is typical of them. The components of epoxy binders are not exceptional [52, 163–165]. It should be kept in

mind that the structures of adsorption layers are different for one-dimensional CNTs, two-dimensional graphene, and three-dimensional metal-containing nanoparticles [166]. In the latter case, the agglomeration of particles accompanied by the development of fractal structures possessing peculiar adsorption properties is possible [12].

CNTs and graphene can be noncovalently functionalized without distortion of the morphological structure through formation of π–π bonds with aromatic compounds and corresponding polymers and surfactants via ionic interactions [163, 164, 167, 168]. The silicate surface of MMT and halloysite nanoparticles ([169]) is modified with organic compounds, including amines and silanes [113, 170]; in this case, ionic bonds may form.

Alkylamine-type compounds react with the nanoparticles of metals and their oxides to form Mt–N bonds [165, 171, 172]. The same behavior is typical of alkylthiols. But if S–Mt bonds exist, the potential of attraction between the alkyl chain and the surface of nanoparticles is such that adsorbed molecules form bonds with the maximum possible number of surface metal atoms [173].

At the same time, the molecular dynamic calculations of the surface area σ_r of alkanethiols adsorbed by a spherical gold nanoparticle [174] showed that σ_r declines with decrease in radius r according to the following formula:

$$\frac{\sigma_r}{\sigma_f} = \left(1 + \frac{0.8}{r}\right)^{-1}, \quad (5)$$

where σ_f is the footprint of an alkanethiol molecule on the flat surface and r is expressed in nm.

It was shown that, beginning from hexanethiol, the value of σ_r is independent of the ligand length. Calculations are consistent with the experimental data [175].

Thus, adsorption is a cause of interfacial layer formation.

Another factor ensuring the stable interfacial interaction of nanoparticles with a matrix is their covalent functionalization [30, 176, 177]. It should be noted that, as opposed to noncovalent modification, covalent modification may introduce defects into the structure of nanoparticles. For example, the introduction of surface COOH groups via the oxidation of CNTs leads to bending of the tube and thus worsens its mechanical and conducting properties [178].

Finally, the specific feature of epoxy nanocomposites, namely, that the synthesis of the epoxy matrix occurs as a rule at elevated temperatures and the resulting material is exploited at room temperature should be taken into consideration. Because of a difference in thermal expansion coefficients of a filler and a matrix, the interfacial layer may be deformed to a certain extent.

The glass-transition temperature T_g characterizes the matrix, because it is a function of its molecular architecture and depends on such parameters as the functionality of an epoxy oligomer and curing agent and the degree of conversion. Research into the processes of curing of the matrix in the presence of nanoparticles shows (above) that an unambiguous conclusion about their effect on T_g is hardly possible. A. Allaoui and N.-E. El Bounia [179] analyzed the published data and inferred that, if single-wall CNTs can cause a decrease in T_g because of their tendency toward aggregation, then multiwall CNTs are inclined to increase or not change T_g of epoxy nanocomposites. However, K.W. Putz et al. [180] demonstrated that the effect of multiwall CNTs (0.25 and 0.5%) on T_g depends on the density of the matrix network: in loosely crosslinked networks, T_g grows, while in densely crosslinked networks, T_g decreases. It is supposed that the interfacial interaction plays the decisive role in these cases. In loose networks, a filler restricts the mobility of kinetic fragments owing to their adsorption, while in dense multiwall CNTs it hampers formation of network junctions.

Formation of interfacial layers both in the absence of covalent functionalization and in its presence was proved in [181]. Single-wall and multiwall CNTs were treated with a mixture of nitric and sulfuric acids; as a result, carboxyl groups appeared on the surface. The latter were transformed into ester groups through the reaction with phenyl glycidyl ether. The matrix was obtained by the curing of BADGE with poly(ether triamine). The difference in the treatment procedure is reflected in the structure of the interfacial layer, as manifested by relaxation spectra. As evidenced by the pattern of tan $\delta(T)$ curves obtained at a frequency of 0.1 Hz (Fig. 6), a high-temperature transition typical of the matrix (curves *1*) is registered for composites based on both single-wall CNTs and multiwall CNTs. But in the case of unmodified (curves *2*) and COOH-modified (curves *3*) CNTs, an additional transition is observed at a lower temperature.

This finding indicates the presence of a structure that is less perfect than the structure of the matrix and is apparently localized in the interfacial layer. The authors believe that the observed effect is associated with the selective adsorption of an epoxy oligomer on tubes, which is hardly possible when ester fragments occur on the surface (curves *4*). Another explanation of this effect is also possible: ester tails facilitate the relaxation of stress of the interfacial layer.

Note that, in the case of single-wall CNTs, the effect is more pronounced than that for multiwall CNTs. This is the evident consequence of the fact that single-wall CNTs are modified to a higher extent (8.6% versus 4.9% with respect to carboxyl groups and 21.1% versus 13.7% with respect to ester fragments).

S. Wang et al. [182] estimated the shear strength of the interface single-wall CNT/epoxy matrix as

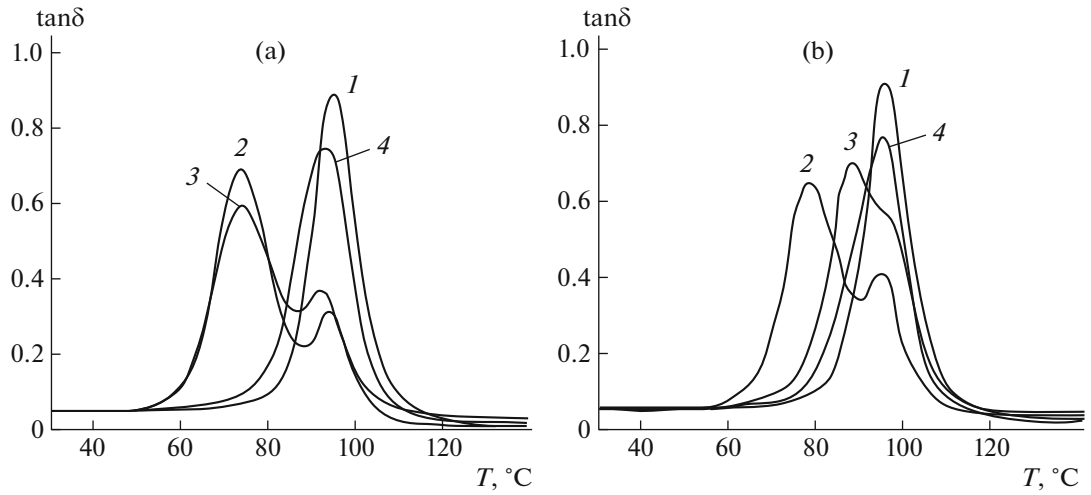

Fig. 6. Temperature dependence of tan δ of epoxy matrices and epoxy nanocomposites containing 1 wt % of (a) single-wall CNTs and (b) multiwall CNTs. (*1*) The neat resin and (*2*–*4*) the epoxy nanocomposite with (*2*) unmodified nanoparticles and nanoparticles modified with (*3*) COOH groups and (*4*) grafted ester fragments. The data are taken from [181].

306 MPa under the assumption that tubes are not clustered and that the grafting of diethyltoluenediamine leads, on average, to formation of one bond per 25 carbon atoms. In accordance with the same calculations, the strength of the interfacial layer in the case of unmodified single-wall CNTs is ~50 MPa. However, it should be borne in mind that the strength of the interfacial layer τ depends on the radius of CNTs. For example, according to the data [183] obtained by the method of pulling from the polyethylenebutylene matrix, τ ≈ 85 MPa for multiwall CNTs with a radius of 10–20 nm and it drops to ~15 MPa at 60–70 nm.

A number of methods for the covalent modification of CNTs and manifestation of their functionalization in the properties of epoxy nanocomposites are discussed in reviews [22, 30, 184]. In [167, 185–187], methods used for functionalization of graphene are described which in principle do not differ from those used in previous cases. For example, the dispersion of graphene in a mixture of methylsulfonic acid and P_2O_5 was acylated by dicarboxylic acid (4,4'-dicarboxydiphenyl ether) and then the polycondensation reaction with 3,3'-diaminobenzidine was performed in situ to afford the graft polybenzimidazole [184]. As in the case of CNTs, an important circumstance is the disaggregation of graphene sheets [188] taking into consideration that the latter shows the tendency toward aggregation in the epoxy matrix.

As an initial reagent in covalent functionalization, graphene oxide (GO) is often used, which is obtained, in particular, by the oxidation of graphite.

Amino and epoxy-functionalized GO were synthesized using silane binding agents: 3-aminopropyltriethoxysilane and 3-glycidoxypropyltrimethoxysilane [189].

Alkylamines consisting of long-chain hydrophobic alkyl groups and hydrophilic amino groups are grafted onto the surface of GO owing to the presence of two types of reactive groups on it, namely, carboxyl and epoxy. The former groups are involved in the amidation reaction, while the latter groups participate in the nucleophilic substitution reaction [190]. The use of bifunctional poly(ester diamine) makes it possible to graft amino-containing fragments able to react with the epoxy groups of a binder [191]. Molecules with different chain lengths were used (D230 and D2000). It was assumed that different interface structures between a filler and a matrix will be created. The grafting of D230 chains onto the surface of GO leads to the restricted mobility of segments and, accordingly, to the minimum deformability. D2000 chains feature a much higher deformability because of their higher length. This promotes a rise in mobility of the filler in the matrix and causes scattering of energy during deformation. As a result, the interphase obtained using D230 and D2000 leads to difference in the mechanical properties of the nanocomposites.

R. Konnola et al. [192] using relationship (6) estimated the volume fraction of the interphase v_{int} in the epoxy nanocomposites in which the neat GO and GO with the grafted copolymer of acrylonitrile and butadiene were used as fillers.

$$\tan\delta = \frac{\tan\delta_m}{1 + B\varphi}. \quad (6)$$

Here tan δ and tan δ_m are the values of loss tangent of the nanocomposite and matrix with the volume fraction of the filler φ, and B is a parameter which in essence characterizes the volume of the interfacial layer [193]: $B = 1 + (\Delta R/R_0)^3$, where R_0 is the radius of

a nanoparticle and ΔR is the thickness of the interfacial layer.

Calculations showed that, for a filler concentration of 0.6 wt %, the corresponding values of v_{int} are 0.0040 and 0.0114.

As was mentioned above, in MMT, the intercalation of various compounds is feasible [95, 96], which after exfoliation of the filler form in fact the interfacial layer. With this aim in view, L. Yang et al. [194] used 2-(3,4-dihydroxyphenyl)ethylamine, which was involved in oxidative polymerization [194, 195], and the surface of MMT was covered by the resulting polymer. The interlayer distance increased during polymerization.

In [196], epoxy nanocomposites were obtained on the basis of bentonite that was modified with diphenylamine-4-diazonium via ionic exchange. The interfacial layer was formed by the oxidative polymerization of aniline. The aryl groups of diazonium strongly affected interfacial interaction as a means of effective stress transfer.

In recent years, composites with halloysite nanotubes have attracted progressively growing attention of researchers [170, 177, 197, 198]. Halloysite is kaoline rolled up to multiwall tubes with an external diameter of nearly 50 nm, an internal diameter of ~15 nm, and a length from 700 to 2000 nm. Composites on their basis can retain and dose for a long time chemical reagents and biologically active compounds (bactericides, antibiotics, and other drugs). Additives to various polymeric materials impart to them desirable mechanical properties while preserving their low density [199]. It is evident that interfacial interaction play not the last role here.

The specific feature of the chemical structure of halloysite nanotubes is that their internal surface is covered by Al–OH groups, whereas the external surface is mostly composed of siloxane groups Si–O–Si. Hence, it follows the strategy for modifying halloysite nanotubes aimed at creating the optimal interfacial layer: the grafting of silanes is a general and efficient procedure for covalent functionalization [177].

Indeed, P. Sun et al. [200] successfully grafted 3-aminopropyltriethoxysilane onto the surface of halloysite nanotubes which was preliminarily treated with a mixture of H_2SO_4 and H_2O_2 in order to increase the concentration of hydroxyl groups having a higher activity with respect to silanization.

As regards metal nanoparticles, as was noted above, adsorption frequently leads to the formation of chemical bonds [173]. For example,

$$RSH + Au_n(0) \rightarrow RS^-Au^+–Au_{n-1}(0) + 1/2H_2;$$

that is, in essence chemisorption occurs. The assorbed molecules may form layers, whose structure depends [199] on the concentration and nature of sorbates (e.g., alkanethiols with the number of CH_2 groups below nine are incapable of self-assembly [201]), temperature, and sorbent. For example, molecular mechanics studies of A.P. Kaushik and P. Clancy [202] demonstrated that small (3 nm) and coarser (6 nm or above) particles behave in a different manner because of different conformations of ligands on their surface. The length of the ligand is comparable with the lateral sizes of the facets of small metal-containing nanoparticles. These molecules try to maximize interaction with facets and, hence, prefer to occupy the horizontal position with respect to the facet. As a result, ligands on small metal-containing nanoparticles are, as a rule, localized via twisting around the core. Ligands on coarse particles having a greater number of ligands on the surface contact each other and decrease the possibility of interaction with a metal core. Owing to presence of a large number of ligands on the surface, their horizontal position on core facets is hardly probable because of steric hindrances and, therefore, they should orient vertically. Naturally, the interfacial interaction of the matrix with metal-containing nanoparticles will also depend on their size.

Mechanical Properties

The use of nanoparticles as reinforcing agents for epoxy polymers assumes solution of tasks common for polymeric composite materials, namely, dispersion of agglomerates and assurance of stress transfer from the matrix to the filler owing to creating corresponding interfacial interaction. This requires that the chemism of the curing processes of the epoxy binder and the chemical and physical structures of the formed matrix be taken into consideration.

Moreover, the dimension of nanoparticles should be taken into account: one-dimensional, two-dimensional, and three-dimensional fillers.

One-dimensional fillers: carbon and halloysite nanotubes. CNTs and halloysite nanotubes may be regarded as fibers of finite length.

Mechanical properties, and not only they, depend on both the degree of filling and the aspect ratio (in what follows aspect) χ—the length-to-diameter ratio. For example, in the case of unidirectionally oriented fibers at a low volume filling, the Young modulus of the composite in the direction of orientation E_{11} is expressed through the ratio [203]

$$\frac{E_{11}}{E_m} = \varphi_f A, \quad (7)$$

where E_m is the modulus of the matrix and φ_f is the volume fraction of the fiber. Parameter A is a function of the longitudinal modulus E_f and the fiber aspect χ, as depicted in Fig. 7.

At high values of fiber modulus (the plateau region on the curves), the value of parameter A is primarily determined by just the aspect. In the case of chaotic

orientation of fibers, the modulus of the composite E_c may be presented as follows [204]:

$$E_c = \frac{3}{8}E_{11} + \frac{5}{8}E_{22} \quad (8)$$

The transverse modulus E_{22} at a low filling may be calculated through the mix formula

$$E_{22} = \frac{E_{tr}E_m}{E_{tr}\varphi + E_m(1-\varphi)}. \quad (9)$$

Here E_{tr} is the transverse modulus of a fiber and E_m is the modulus of the matrix, with $E_{tr} \ll E_m$.

From formulas (7)–(9) it follows that

$$\frac{E_c}{E_m} = \frac{1}{8}\left(5 + \varphi_f\left(3A + 5\frac{E_{tr}}{E_m} - 5\right)\right) \approx \frac{5}{8}(1-\varphi_f) + \frac{3}{8}\varphi_f A, \quad (10)$$

that is, the main contribiution to the value of the modulus is provided by parameter A. As is seen from formula (10) and Fig. 7, at a low filling ($\varphi_f < 0.01$), the efficiency of the fiber becomes apparent only at $\chi \gg 10$.

In the ideal case (the Kelly model), the strength of composite σ_c obeys the mix rule [203]

$$\sigma_c = \eta\xi\left(1 - \frac{\sigma_f}{2\chi\tau}\right)\sigma_f\varphi_f + \sigma_m(1-\varphi_f), \quad (11)$$

where σ_f and σ_m are the strength of the fiber and matrix, η is the orientation factor equal to 0.2 for the random distribution of fibers over directions [205], ξ is the coefficient allowing for the level of realization of fiber properties, and τ is the shear strength of the interfacial layer.

Formulas (10) and (11) describe the ideal situation. In most studies, the experimental data are matched to the Tsai–Halpin equation [206, 207]:

$$\frac{E_c}{E_m} = \frac{1}{8}\left(3\frac{1+2\chi\eta_l\varphi_f}{1-\eta_l\varphi_f} + 5\frac{1+2\eta_t\varphi_f}{1-\eta_t\varphi_f}\right) \quad (12)$$

$$\left(\eta_l = \frac{E_f - E_m}{E_f + 2\chi E_m}, \quad \eta_t = \frac{E_f - E_m}{E_f + 2E_m}\right)$$

M. Ayatollahi et al. [207] used formula (12) to interpret the obtained dependence of the modulus of the epoxy nanocomposite on concentration (0.1, 0.5, and 1 wt %) and aspect (from 455 to 1000) of multiwall CNTs; the value of χ was changed via variation in diameter rather than length. These authors showed that satisfactory agreement between the experimental data and calculations may be attained setting $\chi \to a\chi^b$, $a = 0.0488$, and $b = 1.141$. It is supposed that this makes it possible to allow for the imperfection of interfacial interaction, agglomeration, and other possible drawbacks of the model (12).

With increasing aspect, the strength and fracture toughness of the epoxy nanocomposite increased.

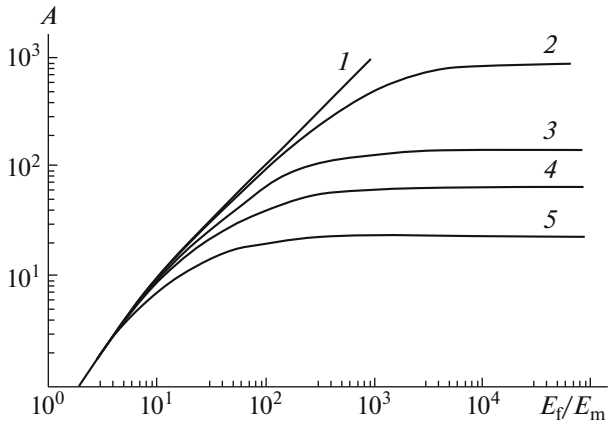

Fig. 7. Dependence of the Young modulus of the unidirectional composite (parameter A) on fiber characteristics. $\chi^{-1} = 0$ (*1*), 0.01 (*2*), 0.03 (*3*), 0.05 (*4*), and 0.10 (*5*). The data are taken from [203].

However, as was shown above, the growth of χ is related to a decrease in diameter. In accordance with [183], particles with a smaller diameter create a stronger interfacial interaction with a matrix. This facilitates load transfer and, accordingly, improves mechanical properties.

A number of models taking into consideration the effect of curvature of CNTs on the properties of the material were considered in [208–212]. For example, the authors of [210] advanced a new expression for the rule of mixtures

$$\frac{E_c}{E_m} = \frac{(k_1 k E_f - E_m)\varphi_f}{E_f - (E_f - E_m)\varphi_f}, \quad (13)$$

where $k_1 = 1 - \frac{\tanh(2\chi\tau)}{2\chi\tau}$, $\tau = \sqrt{\frac{-2E_m}{E_f(1-\mu)\ln\varphi_m}}$,

Here μ is the Poisson coefficient of the matrix; k is the empirical constant allowing for the orientation and curvature of CNTs. The authors managed to choose the values of $k < 1$ describing the experimental data on the moduli of the epoxy nanocomposite via Eq. (13). The same considerations are used to interpret the experimental data on strength.

But the researchers mostly use the modified Eq. (12)

$$\frac{E_c}{E_m} = \frac{1+2\chi\eta\varphi_f}{1-\eta\varphi_f} \quad (12a)$$

$$\left(\eta = \frac{E_f - E_m}{E_f + 2\chi E_m}\right).$$

It is believed [212] that, owing to replacement $\chi \to \chi\exp\{-a-b\varphi_f\}$, the curvature of multiwall CNTs may be taken into consideration (Fig. 8).

The strongest effect on the mechanical properties of a nanocomposite is affected by the functionaliza-

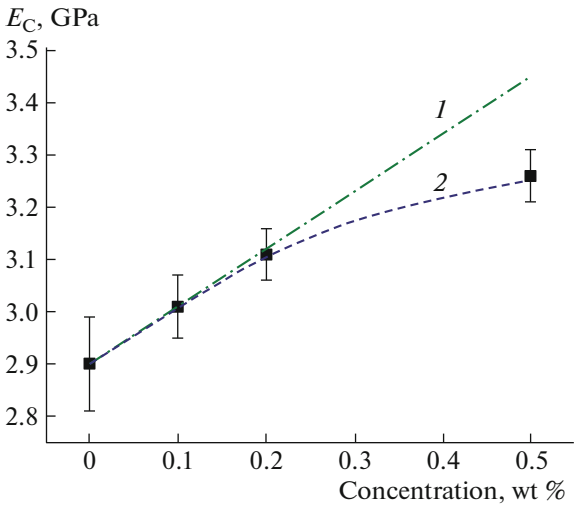

Fig. 8. Dependence of the elastic modulus of the epoxy nanocomposite on the concentration of multiwall CNTs (closed squares). (*1*) Eq. (12a) and (*2*) Eq. (12a) with correction for curvature $a = 9.15$ and $b = 0.12$. The data are taken from [212].

tion of CNTs. For example, the modulus of epoxy nanocomposites containing 3% of untreated multiwall CNTs or multiwall CNTs functionalized through treatment with a mixture of aminobenzoic and polyphosphoric acids increased by 32 and 53%, respectively [68]. Note that the glass-transition temperature also increased somewhat: 189 (matrix), 190, and 199°C.

X. Chen et al. [213] showed that the ultimate tensile strength of the epoxy nanocomposite (1.5 wt % filler) grows from 39 MPa (matrix) to 46 in the case of untreated multiwall CNTs and to 59 MPa for multiwall CNTs functionalized by amino groups. The glass-transition temperature also grows from 98 to 109 and 112°C.

The behavior of epoxy nanocomposites depends not only on the type of functional groups but also on the structure of molecules grafted onto the surface of CNTs. For example, in [214], double-wall CNTs (with admixture of single-, three-, and multiwall CNTs), which were initially treated with acid, entered into the reaction with diamines: 1,12-diaminododecane (1), 7,10-trioxa-1,13-tridecanediamine (2), and 4,4'-(4,4'-methylene-bis(4,1-phenylene)-bis(methylene))dianiline (3). Epoxy nanocomposites containing 0.1 wt % of double-wall CNTs had the following values of shear modulus G' ($T < T_g$): 989 (1), 993 (2), and 1393 MPa (3), whereas for the matrix $G' = 731$ MPa.

In [177], the functionalization of halloysite nanotubes was performed using 3-(2-aminoethyl)aminopropyltriethoxysilane, (3-glycidyloxypropyl)trimethoxysilane, or octyltriethoxysilane to afford grafted amino and epoxy groups and the functionless "tail." The corresponding composite materials containing 2.5 or 5.0 wt % of the above nanoparticles had $G'(50)$ and $G'(200)$ at a level or slightly above those of the initial matrix, with T_g being unchanged (173–176°C).

According to general ideas, functionalization facilitates the dispersion of nanotubes in a matrix. For example, in accordance with [215], amino-functionalized CNTs have a higher surface energy than the unmodified CNTs and their wettability by the epoxy resin is much better, and the grafted amine molecules arising as a result of functionalization efficiently inhibit the repeated agglomeration of CNTs during resin curing. However, functionalization also enhances adhesion at the interface CNTs/epoxy resin, thereby improving mechanical properties of the matrix. In essence, the problem is reduced to formation of the interfacial layer (see the previous section) and its role in controlling properties of the composite material.

Using scanning electron microscopy N. Lachman and H.D. Wagner [216] studied the fractured surfaces of epoxy nanocomposites after pulling of multiwall CNTs. The diameter of a footprint from the removed tube was regarded as a marker of epoxy adhesion. It was found that the diameter of the unmodified multiwall CNTs is slightly above the diameter of nanotubes, whereas in the case of carboxyl- and amino-functionalized multiwall CNTs the diameter of the footprint is several times higher. These data are in agreement with the results of mechanical testing of the nanocomposites.

Thus, formation of the interfacial layer is responsible for the reinforcement of nanocomposites.

Moreover, when analyzing the effect of low concentrations of the filler, one cannot but allow for contribution of the matrix to the mechanical properties of composites, the structure of which changes because of the impact of nanoparticles on its formation. The catalytic effect of surface groups leads to the frontal autocatalytic reaction (Fig. 3), which results in the heterogeneous microphase structure of the polymer (Fig. 9) [71].

Owing to the existence of regions with different packing densities in the polymer (this hampers crack propagation under loading), the energy of viscous destruction rises, elongation at break grows, and, accordingly, the strength of the samples increases. Therefore, it is evident that classical additivity formulas are of limited use for calculating the physicomechanical parameters of nanocomposites.

Two-dimensional fillers: graphene and MMT. For two-dimensional sheets, aspect χ as the ratio of diameter to thickness should also be taken into account.

The authors of [217] developed a method (references in [217]) for estimating the value of χ from the viscosity of dilute suspensions according to the Einstein equation

$$\eta_r = 1 + k_1\varphi,$$

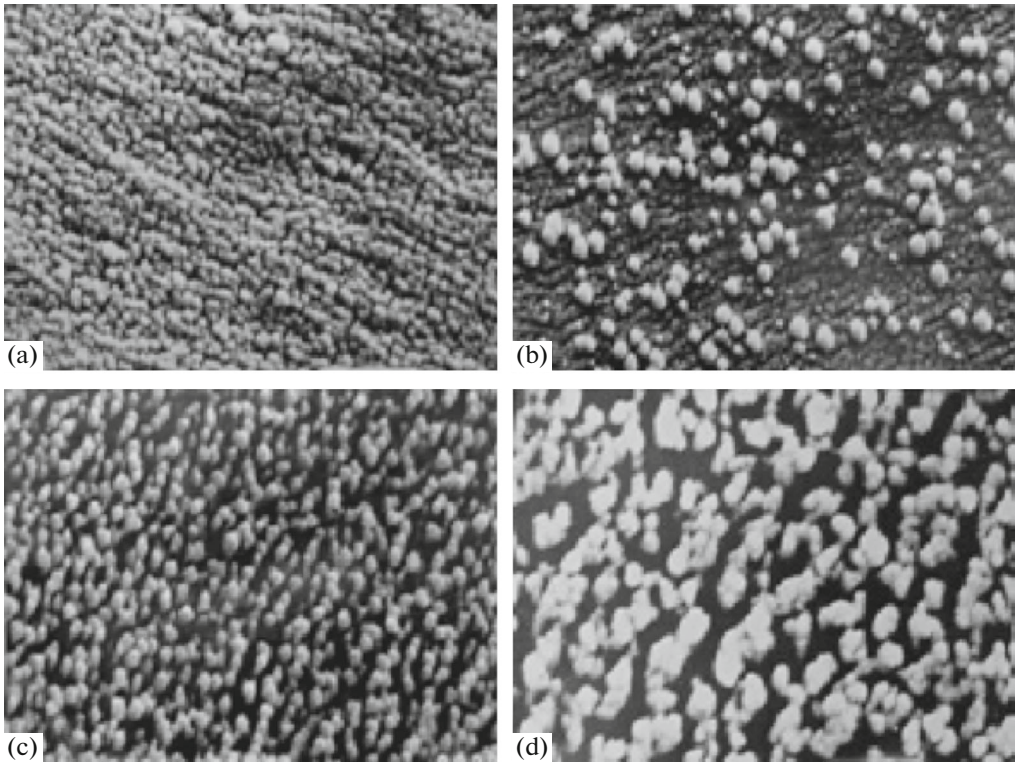

Fig. 9. SEM microimages of epoxy composites with content of carboxylated multiwall CNTs of (a) 0, (b) 0.01, (c) 0.10, and (d) 0.5 wt %. Magnification of 20 000×. The data are taken from [71].

where η_r is the relative viscosity, φ is the volume fraction of suspension ($\varphi < 0.02$), and coefficient $k_1 = \frac{\chi}{2\ln(2\chi) - 3} + 2$.

The authors investigated two kinds of graphene which were obtained using different technologies. The elastic modulus of the composite material was calculated according to Eq. (12a) except that formula (8) was changed for the following one:

$$E_c = \frac{1}{5}E_{11} + \frac{4}{5}E_{33}, \quad (8a)$$

and $E_{11} = E_{22}$ and E_{33} was obtained via expression (12a). It was assumed that $\chi = 2$ for E_{33} and the value of χ was a fitting parameter for E_{11}. E_f was calculated via formula (8a), where E_{f11} was in the range of 250–1000 GPa and $E_{f\,33} = 50$ GPa.

Figure 10 presents the results of the mechanical testing of epoxy nanocomposites based on graphene. As is clear, these data are satisfactorily described by Eq. (12a). The fitting value of $\chi = 1000$ is close to the value calculated from the rheological measurements: ~1250.

X. Wang et al. [218] explored the effect of graphene size on the mechanical properties of the epoxy nanocomposite (Fig. 11). GO samples 1, 2, and 3 had conditional sizes of 10.79, 1.72, and 0.70 μm.

It is known that, in the case of CNTs, the smaller the diameter, the stronger the effect ([22]). This is primarily related to the fact that the value of specific surface is inversely proportional to radius. However, for two-dimensional graphene sheets, this relationship is absent.

In fact, as shown in Fig. 11a, the elastic modulus of the composite is almost insensitive to the size of the filler. As regards fracture toughness, the situation is different (Fig. 11b): the stress concentration coefficient K_{1c} grows with a decrease in size. K_{1c} related to the size of graphene nanoparticle is of critical importance for a rise in impact strength. Graphene sheets in the epoxy matrix disturb crack propagation and prevent their extension. In accordance with [218], they behave as bridge particles that serve as rods linking crack faces. Therefore, their numerical concentration (the smaller the particle size, the higher the numerical concentration) becomes of importance.

As was shown in [219], graphene is more effective than CNTs for improving the mechanical properties of epoxy nanocomposites. For example, at a concentration of 0.1 wt %, the value of K_{1c} grows by 14% for single-wall CNTs, by 20% for multiwall CNTs, and 53% for graphene compared with the matrix.

Comparative data on the tensile testing of epoxy nanocomposite with multiwall CNTs and graphene are summarized in Table 1 [220]. It is seen that

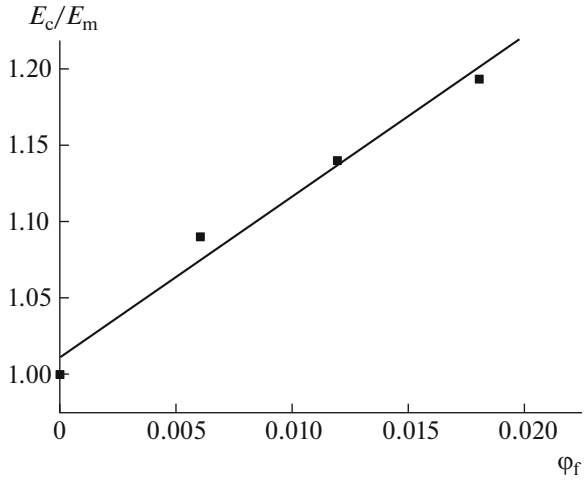

Fig. 10. Dependence of the elastic modulus of the epoxy nanocomposite on the concentration of graphene. Points refer to experiments, and the straight line refers to Eq. (12a), where $E_{f11} = 1000$ GPa and $\chi = 1000$. The data are taken from [217].

graphene imparts rigidity to the composite to a higher extent than multiwall CNTs: the modulus is higher and the strength is lower in correlation with reduction in elongation before break.

In general, in the case of polymer nanocomposites, graphene is superior to CNTs in terms of rheological, thermal, and mechanical properties. This circumstance may be attributed to the two-dimensionality of graphene and its higher specific surface. As a consequence, in the case of graphene, the interphase zone is more extensive and the interfacial interaction of the filler with the polymer matrix is stronger, whereas CNTs may interact with polymers only via one-dimensional linear contacts [221].

X. Tang et al. [222] used triglycidyl-*p*-aminophenol as an agent of transfer of graphene oxide nanoparticles from water to BADGE. Triglycidyl-*p*-aminophenol is adsorbed on the surface of GO, and its sheets exfoliate without any other chemical treatment and are randomly distributed in the epoxy matrix. In addition, triglycidyl-*p*-aminophenol is an efficient modifier of the GO surface enhancing interfacial interaction in the composite. As a consequence, the mechanical properties of the epoxy nanocomposites are improved (Table 2).

It is seen that the filler itself promotes an increase in modulus, but the strength decreases in correlation with a decrease in elongation at break (lines 1, 2). In the presence of triglycidyl-*p*-aminophenol all parameters, including ε, grow (lines 3, 4, 6). Lines 6–8 demonstrate that the dependence of mechanical properties of the epoxy nanocomposite on the concentration of GO follows a nonmonotonic pattern, with the optimum being at 1%.

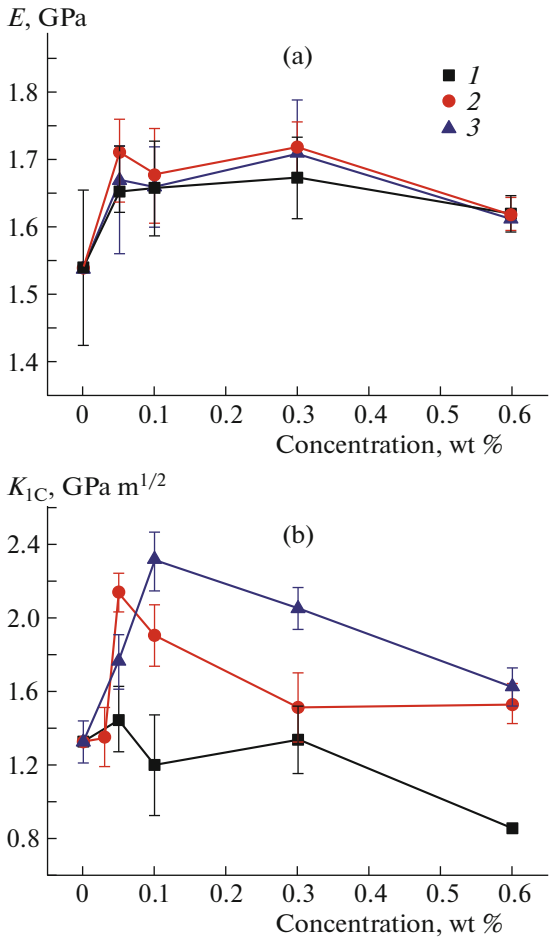

Fig. 11. (Color online) Dependence of (a) elastic modulus and (b) fracture strength on concentration. The sizes of graphene nanoparticles are (*1*) 10.79, (*2*) 1.72, and (*3*) 0.70 μm. The data are taken from [218].

In [75], graphene was obtained from graphite powder by the chemical method and was then functionalized by treatment with the mixture of 4-aminobenzoic and polyphosphoric acids. The epoxy nanocomposites contained 1 wt % graphenes.

Figure 12 shows the relaxation characteristics measured at a frequency of 1 Hz and G' and tan δ values for the matrix and the epoxy nanocomposites containing neat and amino-functionalized graphenes. As is seen, at temperatures below T_g, the modulus of composites grows compared with the matrix and functionalization ensures a more pronounced increase in G'. As follows from tanδ measurements, T_g shows the same tendency.

In [223], the mechanical properties of epoxy nanocomposites were improved via the amino functionalization of graphene nanoparticles which was performed through treatment of its COOH modification with the butadiene and acrylonitrile copolymer containing terminal amino groups. As regards modulus, a

Table 1. Mechanical properties of reinforced nanocomposites: the Young modulus E, breaking stress σ, and elongation at break ε [220]

Material	Concentration, wt %	E, GPa	σ, MPa	ε, %
Matrix	0	1.63	59	5.9
Multiwall CNTs	0.25	1.95	68	5.4
	0.50	2.00	69	4.8
	0.75	2.27	72	4.9
	1.50	2.04	75	5.7
Graphene	0.25	2.16	65	4.3
	0.50	2.30	64	3.8
	0.75	2.39	68	3.7
	1.50	2.47	69	3.7

small increasing effect was observed (Fig. 13a). In contrast, the fracture toughness considerably increased with filling, especially in the case of amino-functionalized graphene (Fig. 13b).

Graphene oxide possesses a chemically active surface owing to the presence of hydroxyl, carboxyl, carbonyl, and epoxy groups [224]. This circumstance makes it possible to expect that GO will exhibit reinforcing ability. In addition, GO may be functionalized via the reaction of these groups. In [186], graphene oxide was modified with 3-glycidoxypropyltrimethoxysilane, while the authors of [187] used BADGE for this purpose. Table 3 lists the mechanical properties of the epoxy matrix and the corresponding composites. It is clear that the epoxy polymer becomes rigid upon the addition of GO and the functionalization of GO enhances this effect. A low concentration of the additive is used. As the concentration increases, the modulus grows, but the strength declines, correlating with reduction in the elongation at break. This tendency seems to be typical ([222, 225]).

Y. Ni et al. [226] managed to overcome this tendency when they designed a three-dimensional framework composed of GO sheets. The aqueous solution of poly(amide amine) (dendrimer) was mixed with the GO suspension at a mass ratio of 1 : 1. This mixture was rapidly frozen in liquid nitrogen and lyophilized. Heating of the resulting porous body at 150°C led to the amidation and reduction of GO. As a result, a three-dimensional graphene product 3DG with a specific surface area of ~200 m^2/g was produced and used for reinforcement of the epoxy matrix.

Figure 14 shows stress–strain curves of the matrix and the epoxy nanocomposites with GO and 3DG. The modulus and strength of the composites (curves *2–4*) are higher than those of the matrix (curve *1*), while the ultimate elongation is lower. When GO is used as a filler, the mechanical parameters are better at 0.1% (curve *3*); their worsening at 0.2% (curve *2*) corresponds to the above-described tendency. The best parameters are observed for the composite with the 3DG filler at a concentration of 0.2% (curve *4*).

As was shown in [227], the optimum mechanical properties (ultimate tensile strength, ultimate flexural strength, impact resistance, and fracture toughness) of the epoxy nanocomposite with MMT additives were reached at 3 wt % and corresponded to increase in these characteristics by 41, 20, 95, and 19% compared with the matrix. This result was explained and verified by the exfoliation of MMT studied by X-ray difraction.

Analogous data were reported by M. Wang et al. [228]: the Young modulus, ultimate strength, and elongation at break, as well as K_{1c} of the epoxy nanocomposite, had the maximum values at an MMT concentration of 1 wt %. These values are higher than the respective parameters of the matrix by 5, 38, 64, and 93%, respectively.

In accordance with [229], the addition of 3 wt % of nanoparticles of MMT, SiO_2, or their mixture (1 : 1, wt/wt) affects the mechanical properties of the epoxy nanocomposite (Table 4). The addition of SiO_2

Table 2. Mechanical properties of epoxy nanocomposites with GO [222]

Material	Concentration of GO, wt %	Concentration of triglycidyl-*n*-aminophenol, wt %	G', GPa (30°C),	σ, MPa	ε, %
Matrix	0	0	2.06	53	5.4
Epoxy nanocomposite	0.5	0	2.26	51	4.8
	1.0	0	2.34	46	4.2
	1.0	5	2.67	57	4.3
	1.0	10	2.75	66	4.8
	0	20	2.12	51	4.4
	0.5	20	2.58	82	5.7
	1.0	20	2.94	101	6.2
	1.5	20	2.84	83	5.0

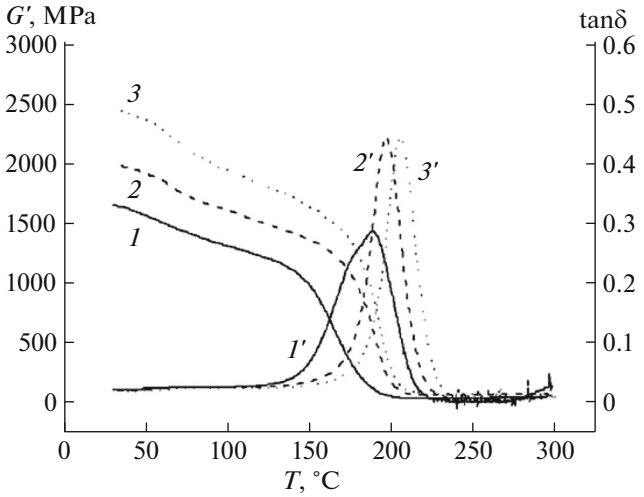

Fig. 12. Real modulus G' (*1*–*3*) and tan δ (*1′*–*3′*) of the matrix (*1*, *1′*) and nanocomposites with (*2*, *2′*) the original and (*3*, *3′*) functionalized graphene. The data are taken from [75].

noticeably increases fracture toughness K_{1c} and tensile strength σ, but the ultimate elongation ε grows slightly. This finding indicates toughening of the matrix. The introduction of MMT, in contrast, promotes increase in ε and σ, but K_{1c} increases insignificantly. All the mentioned parameters appreciably grow upon the addition of mixed nanoparticles MMT + SiO_2. It appears that the difference in the efficiencies of the fillers may be explained by their different shapes.

Actually, SiO_2 are spherical particles, MMT are sheets with an aspect ratio of ~1000, and mixed nanoparticles are complex shaped in the form of sheets with balls attached to them. If the main mechanism of nanocomposite destruction involves the propagation of cracks via exfoliation of the matrix from the nanoparticle, then the synergistic effect of the mixed filler becomes understandable. In this filler, a very complex profile of the surface predetermines elongation of the crack propagation path and increase in the energy of composite destruction.

Three-dimensional fillers: fullerene and metal-containing compounds. Fullerene is of interest as a nanofiller of epoxy nanocomposites because, as opposed to other carbon ingredients, CNTs and graphene, it is three-dimensional and its aspect ratio is unity.

Papers addressing links of the epoxy nanocomposites with the fullerene filler are few in number [230–233]. But in all cases, the observed tendency is as follows: the modulus is weakly sensitive to filling (Fig. 15a); however, even at low fullerene concentrations, the strength parameters of the composite grow considerably.

For epoxy nanocomposites, the main ways to resist destruction are the introduction of particles which could act as rods linking crack faces in a matrix and extension of crack propagation path via branching caused by encounter with nanoparticles and/or its propagation through exfoliation of the matrix. Fullerene particles meet requirements of these mechanisms owing to a high energy of interaction with chain fragments of the epoxy matrix and a high numerical concentration. When the crack interacts with obstacles, its

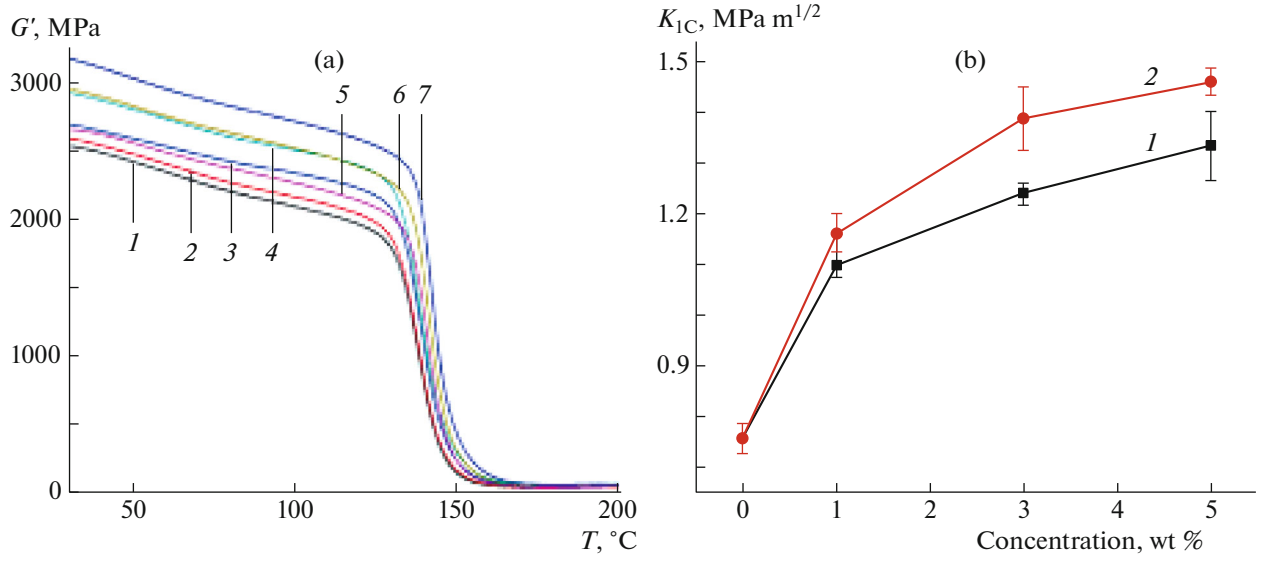

Fig. 13. (Color online) (a) Temperature dependence of the real modulus (at a frequency of 1 Hz) of (*1*) the epoxy matrix and nanocomposites with (*2*–*4*) original and (*5*–*7*) NH_2-functionalized graphene. Concentrations are (*2*, *5*) 1, (*3*, *6*) 3, and (*4*, *7*) 5 wt %; (b) dependence of the fracture strength of nanocomposites with (*1*) original and (*2*) NH_2-functionalized graphene on concentration. The data are taken from [223].

Table 3. Mechanical properties of epoxy nanocomposites with modified GOs [186, 187]

Material	Concentration, vol %	E, GPa	σ, MPa	ε, %	K_{1C}, MPa $m^{1/2}$
Matrix	0	3.15	53	3.75	0.50
Graphene oxide	0.10	3.27	72	4.23	0.59
	0.25	3.32	68	3.85	0.63
	0.50	3.36	65	3.51	0.63
BADGE-functionalized	0.10	3.35	95	6.45	0.68
graphene oxide	0.25	3.56	93	6.32	0.71
	0.50	3.67	85	5.86	0.67
Silane oxide-functionalized	0.10	3.32	81	–	0.69
graphene	0.25	3.46	79	–	–
	0.50	3.60	72	–	–

extension occurs steadily without destruction of the body in a significant load range.

As was shown above, metal-containing nanoparticles should be divided according to the method of their formation: whether they are formed preliminarily, mixed with a binder, and cured in their presence, or they are formed in situ during formation of epoxy nanocomposites. Metal oxides are assigned to the first type, while metals mostly belong to the second type.

Depending on synthesis conditions, the particles of metal oxides have different morphologies and sizes. For example, nanoparticles of iron oxides F_3O_4 synthesized in the presence of surfactants triethanolamine or urea are polygonal or elongated in shape and their average sizes are ~18 or ~39 nm [234]. Accordingly, the properties of epoxy nanocomposites filled with these particles were different.

Figure 16 presents the stress–strain curves for the epoxy matrix (curve *1*) and the epoxy nanocomposites containing 1 wt % of polygonal (curves *2*, *3*) and elongated (curve *4*) F_3O_4 nanoparticles. The latter two particles (*3*, *4*) were treated with 3-aminopropyltrimethoxysilane.

As follows from the above data, fillers insignificantly affect the structure of the polymer because the value of modulus is practically the same for the matrix and the composites. At the same time, the strength grows appreciably and treatment with aminosilane assists in this tendency (curves *2*, *3*). Elongated nanoparticles reinforce composites more efficiently than polygonal nanoparticles (curves *3*, *4*). The value of fracture toughness K_{1c} changes in the same sequence: 0.11, 0.43, 0.62, and 0.89 MPa $m^{1/2}$.

The efficiency of functionalization of metal oxide nanoparticles is confirmed by the data of [235], in which cubic F_2O_3 particles with a size of ~40 nm were treated with 3-aminopropyltrimethoxysilane. The results are summarized in Table 5. As one can see, the strength of the composites grows compared with the matrix. However, the increase in fracture toughness is provided solely by functionalized nanoparticles.

I.A. Al-Ajaj et al. [236] explored how the size of filler particles influences the mechanical properties of the epoxy composite materials using TiO_2 as an example. Nanocomposites (nanoparticles with a size of ~50 nm) and microcomposites (particles with a size of ~50 μm) were compared. The results of three-point bending tests are shown in Fig. 17.

Up to a concentration of 4%, nanoparticles increase all the mechanical characteristics of the composite (Fig. 17, curves *1*). Further reduction is probably associated with the enlargement of particles because of their agglomeration. In the case of microparticles, with increasing concentration, the modulus grows (Fig. 17b, curve *2*), while the strength parameters worsen (Figs. 17a, 17c, curves *2*). This apparently suggests that coarse particles act as stress concentra-

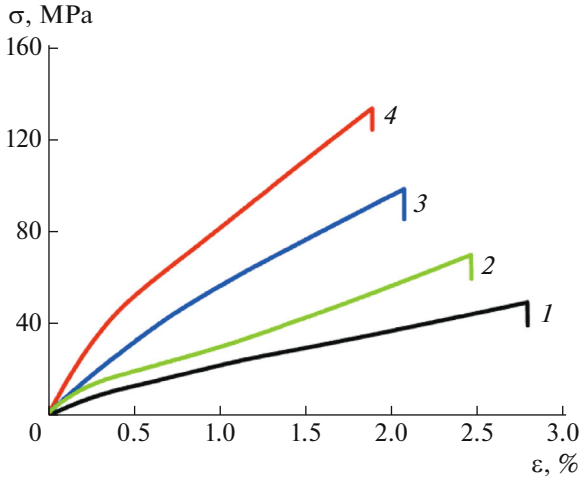

Fig. 14. (Color online) Stress–strain curves of (*1*) the matrix and the epoxy nanocomposites with (*2*, *3*) GO and (*4*) 3DG. Concentrations are (*2*, *4*) 0.2 and (*3*) 0.1 wt %. The data are taken from [226].

Table 4. Mechanical properties of epoxy nanocomposites with MMT/SiO_2 [229]

Material	σ, MPa	ε, %	K_{1C}, MPa $m^{1/2}$
Matrix	58.2	0.49	0.52
Epoxy nanocomposite/SiO_2	87.4	0.76	0.93
Epoxy nanocomposite/MMT + SiO_2	94.9	2.91	1.06
Epoxy nanocomposite/MMT	87.4	3.70	0.56

tors. This circumstance is favorable for destruction of the material. At the same time, at a low concentration, nanoparticles increase the strength of the epoxy nanocomposite via interaction with cracks, as described above.

An example of epoxy nanocomposites with fillers formed in situ is reported in [154]. It was shown that the dependences of the Young modulus E, breaking strength σ, and elongation ε on concentration of the precursor, silver myristate, are described by extremal curves with a maximum corresponding to 0.09 wt %. This result is in sharp contrast with the data presented in the previous paper, where the maximum parameters correspond to 4 vol %, i.e., higher by more than two orders of magnitude. Possibly, this is associated with the sizes of nanoparticles: in the case of Ag, the average radius of nanoparticles is 8.7 nm; for TiO_2, 25 nm.

Electrophysical Properties

For the electrophysical properties of epoxy nanocomposites, the percolation threshold, which depends on the volume concentration, spatial distribution, and aspect ratio of nanoparticles, plays the decisive role along with the electrophysics of fillers.

The percolation threshold. The percolation theory [237, 238] is based on the idea that, as the volume concentration φ grows, nanoparticles are united into clusters of an ever growing size and, when a certain value of φ_c is attained, they form an infinite structure, the so-called percolation cluster. The value of φ_c is the percolation threshold. If nanoparticles are able to conduct electricity, namely, at $\varphi \geq \varphi_c$, the electrical conductivity σ of the composite grows by orders of magnitude. A change in σ appears as a sharp increase in the narrow concentration range of nanoparticles. This allows the percolation transition insulator–conductor to be regarded as a second-order phase transition.

All clusters feature a fractal structure. The "journey" over bonds linking nanoparticles in a finite cluster ($\varphi < \varphi_c$) inevitably leads to terminal branches ("tails"). The percolation cluster ($\varphi \geq \varphi_c$) possesses if only one center linking opposite opposite boundaries of the composite sample, although the amount of "tails" in its structure is more than enough.

In the vicinity of the percolation threshold, dependence σ(φ) is described by the relations

$$\sigma \propto \begin{cases} 0, & \varphi < \varphi_C \\ (\varphi - \varphi_C)^{\beta}, & \varphi \geq \varphi_C \end{cases} \quad (14)$$

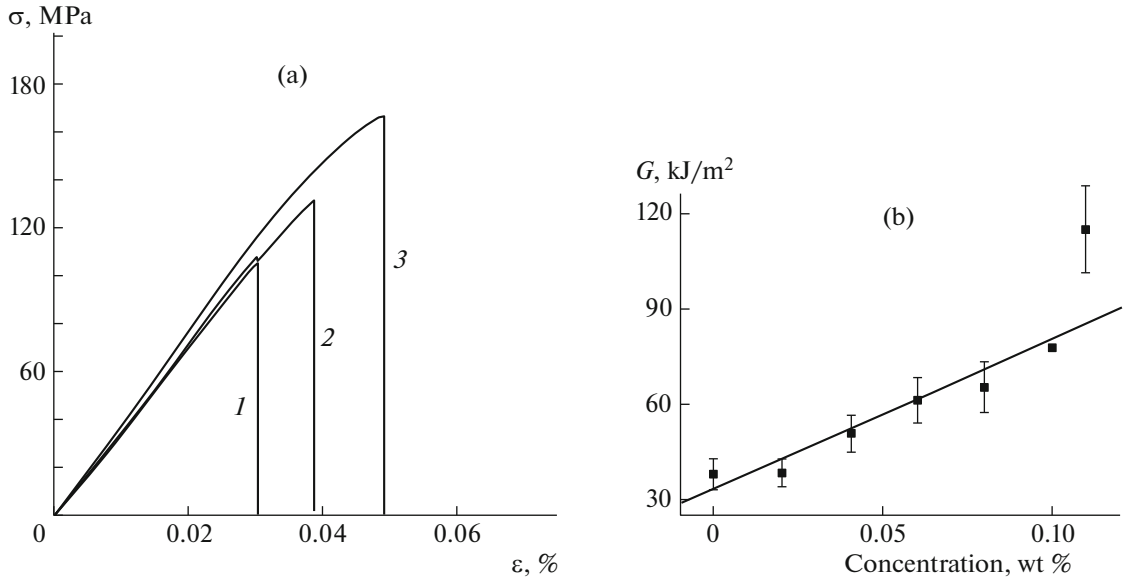

Fig. 15. (a) Stress–strain curves of the matrix and epoxy nanocomposite and (b) the dependence of shock strength of epoxy nanocomposite on the concentration of fullerene. (a) Concentrations of fullerene are (*1*) 0, (*2*) 0.04, and (*3*) 0.1 wt %. The data are taken from [232].

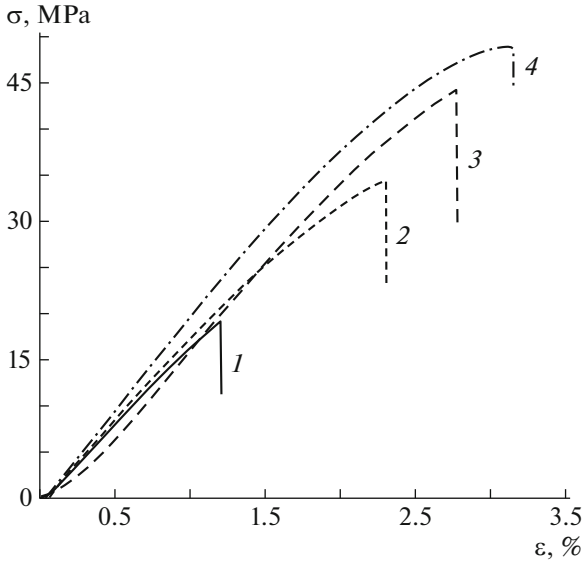

Fig. 16. Stress–strain curves of (*1*) the matrix and the epoxy nanocomposite with (*2*, *3*) polygonal and (*4*) elongated F_3O_4 nanoparticles (*3*, *4*) treated with 3-aminopropyltrimethoxysilane. The data are taken from [234].

For convenience of further presentation, it is useful to introduce the idea of the correlation length (characteristic size) of the finite cluster ξ:

$$\xi \propto (\varphi_c - \varphi)^{-\nu}, \quad \varphi < \varphi_C \tag{14a}$$

Parameters β and ν are called critical parameters.

Naturally, the percolation threshold depends on the structural characteristics of nanoparticles. Figure 18 presents the data reported by J. Li et al. [239] on the effect of the degree of dispersion and the aspect ratio χ of particles on the value of φ_c. These authors examined the behavior of cylindrical nanoparticles with length *l* and diameter *d* and arrived at the equation relating the value of φ_c to the parameters of nanoparticles and the degree of their aggregation ε. The curves refer to calculations via the equation for the values of ε designated by number of the curves on the figure. At aspect ratio $l/d = \chi \sim 100$, the curves describing function $\varphi_c = f(\chi)$ attain a plateau and just aggregation becomes the decisive factor. The lower the aggregation, i.e., the higher the dispersion of particles, the lower the percolation threshold. At the same time, as follows from these data, the value of φ_c is insensitive to the size of nanoparticles at $\chi < 10$. The experimental data on multiwall CNTs are also presented in the figure as open circles [239].

The value of critical concentration φ_c depends not only on such parameters as the size and shape of nanoparticles but also on interaction between them and the matrix. This point may be illustrated by the data of [240] displayed in Fig. 19.

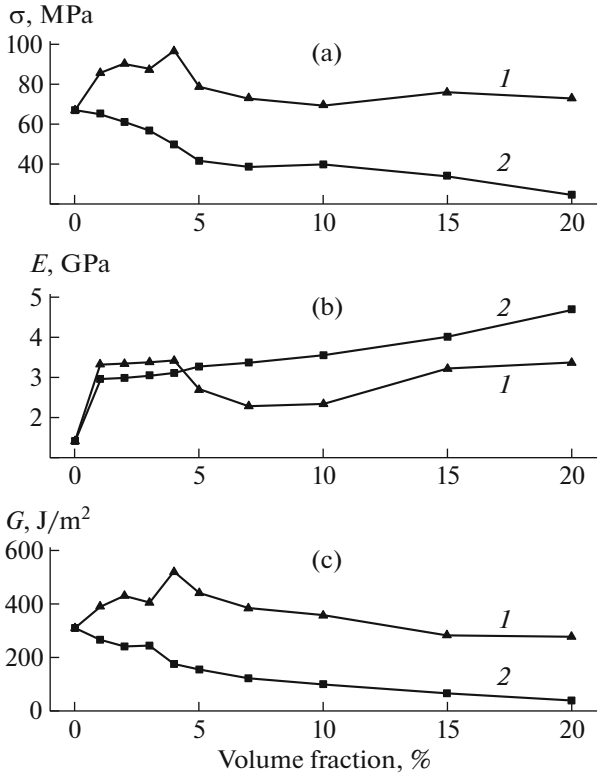

Fig. 17. Dependence of (a) strength, (b) modulus, and (c) fracture energy of the composite on the volume fraction of (*1*) nanoparticles and (*2*) microparticles of TiO_2. The data are taken from [236].

If for nonfunctionalized multiwall CNTs the percolation threshold, as estimated from electrical conductivity, is less than 0.1% (curve *1*), then the introduction of COOH groups that drastically change the character of interaction of tubes with the matrix (section "One-dimensional fillers: carbon and halloysite nanotubes") shifts φ_c far to the right (curve *2*).

These conclusions were varified in [241], in which the authors compared chemically equivalent com-

Table 5. Mechanical properties of epoxy nanocomposites with F_2O_3 [235]

Material	Concentration, wt %	σ, MPa	K_{1C}, MPa m$^{1/2}$
Matrix	0	59.3	1.21
Epoxy nanocomposite without F_2O_3	1	63.2	1.19
	2	67.8	1.16
Epoxy nanocomposite, functionalized by F_2O_3	1	73.6	1.88
	2	78.3	2.06
	3	84.8	2.27
	4	89.1	2.49

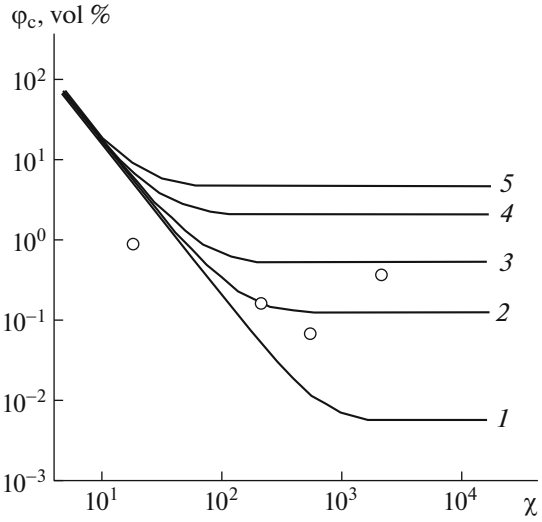

Fig. 18. Relation of the value of φ_c to parameters χ and ε. ε = (*1*) 0.01, (*2*) 0.05, (*3*) 0.1, (*4*) 0.2, and (*5*) 0.4. See text for explanations. The data are taken from [239].

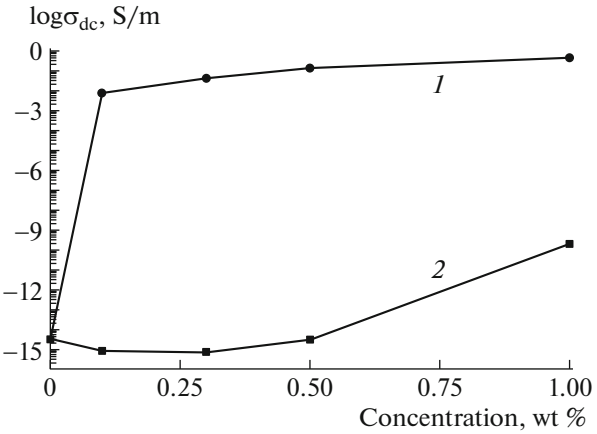

Fig. 19. Dependence of dc conductivity of the epoxy nanocomposite on the concentration of (*1*) original and (*2*) COOH-functionalized multiwall CNTs. The data are taken from [240].

pounds and inferred that covalent functionalization, which is favorable with respect to the mechanical properties of a composite material, by no means improves its conducting characteristics.

Electrical conductivity of epoxy nanocomposites with carbon nanoparticles. CNTs and graphene are anisodiametric particles; therefore, the electrical conductivity of polymeric composite materials will be determined by their aspect ratio, the pattern of orientation, and the degree of dispersion. These parameters will determine the value of the percolation threshold.

The electronic and, hence, conducting properties of CNTs depend on their chirality. The latter appears during the synthesis and characterizes the way of twisting of the graphene plane into a cylinder. The diameter and helicity of the tube are related to chirality. The limiting cases occur in zigzag and chair configurations. The first structure is fully symmetric (the zero chirality), while the second structure is helical at an angle of 30°.

Single-wall CNTs with the zigzag structure are semiconductors, while their chair-type structures are conducting. Multiwall CNTs are always conductors. The macroscopic samples of single-wall CNTs in the form of chaotically arranged bundles feature conductivity up to 10^3 S/cm. However, the specific resistance of the system is determined not so much by the properties of CNTs as contacts between them; that is, the limiting stage of conduction occurs via the hopping mechanism [44–46].

Charge carriers of graphene behave as massless relativistic particles (Dirac fermions). A high electron conductivity in a layer is related to a high quality of its crystal lattice, i.e., low concentration of various kinds of defects that act as scattering sites and inhibit charge transport by means of limitation of electron free path length [47, 48, 242].

Although graphene compared with multiwall CNTs has a higher electrical conductivity (~10^6 S/cm vs. ~10^5 S/cm), the percolation threshold of the latter in polymer composites is much lower: mass percent fractions against 1–2% [221, 243].

The electrical conductivity of composites is usually studied by analyzing the concentration and temperature dependences of dc conductivity σ_{dc} (dc measurements) and the real part of complex ac conductivity σ_{ac} (ac measurements). The data reported in [240] illustrate the first approach [240] (Fig. 19). The second approach was implemented by A. Vavouliotis et al. [244] in the study of the electrical conductivity of epoxy nanocomposites in which multiwall CNTs were used as nanoparticles. The results are shown in Fig. 20.

It is seen that σ_{ac} depends on the frequency and content of multiwall CNTs and grows by almost ten orders of magnitude with increase in these values. The curves of ac conductivity of the matrix and the sample with the lowest concentration almost coincide and show a power-law dependence of σ_{ac} on ω. In the low-frequency range, there is a sharp rise in conductivity (up to eight orders of magnitude) between samples containing 0.1 and 0.3 wt % multiwall CNTs. Nanocomposites with concentrations equal to or above 0.3% demonstrate a broad plateau of the so-called apparent dc conductivity. It appears that the percolation threshold evidently demonstrates itself.

On the basis of the dc conductivity data and using Eq. (14) the critical concentration of multiwall CNTs φ_c and the critical factor β were estimated as 0.089 wt % and 2.574, respectively. For the ac conductivity, the results were as follows: φ_c = 0.098 wt % and β = 3.204.

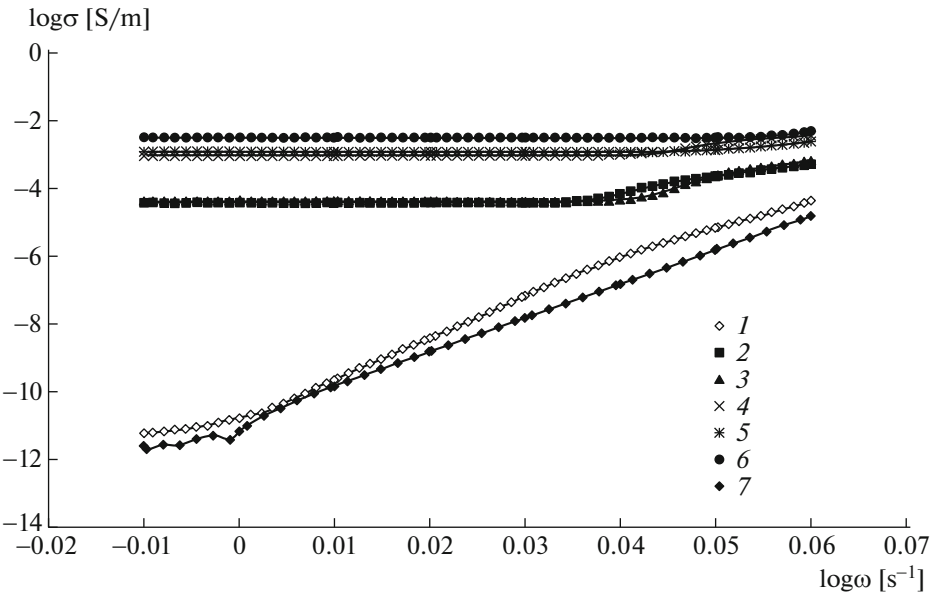

Fig. 20. Dependence of ac conductivity of the epoxy nanocomposite on frequency. The concentrations of multiwall CNTs are (*1*) 0.1, (*2*) 0.3, (*3*) 0.5, (*4*) 0.6, (*5*) 0.8, and (*6*) 1.0 wt %; (*7*) matrix. The data are taken from [244].

This difference may apparently be explained by different conduction mechanisms. The dc conduction is determined via overcoming of energy barriers between favorable conducting regions within the material and formation of a continuous percolation path between electrodes. Charge carriers are forced to migrate over long distances. In addition, in the ac conduction, an increase in frequency causes a reduction in the average shift of current carriers and a rise in σ_{ac}, because a better usage of conducting particles is achieved. The probability of hopping conduction between the latter grows, and the conduction includes contributions of both the continuous path and the existing terminal branches. Thus, in ac measurements, any contact resistances are eliminated and/or decreased at all scale levels of interaction (from sample macroelectrodes to nanotube–nanotube).

G.D. Seidel and D.C. Lagoudas [245] advanced a model for estimating the effect of electron hops and formation of conducting circuits on the electrical conductivity of CNT-polymer nanocomposites owing to the use of a conducting interfacial layer. If well-dispersed CNTs are located in close proximity, then the hops of electrons may occur readily. The critical thickness of the interlayer providing the hopping mechanism of conduction is independent of the diameter *d* of tubes. Note that the higher the *d*, the more pronounced the percolation concentration. For multiwall CNTs, the radius is higher compared with single-wall CNTs, so that the percolation threshold related to the hopping of electrons is much higher. In fact, as was found in [246], in the epoxy nanocomposites with single-wall CNTs, φ_c is about 0.015 wt %; in the case of the CNT mixture, φ_c is about 0.0225.

At high concentrations, the conductivity of the composite material will be determined by the electronic properties of CNTs. But if multiwall nanotubes are conducting, then a certain fraction of single-wall nanotubes are semiconductors. Therefore, at equal concentrations, single-wall CNTs will possess a lower electrical conductivity than multiwall CNTs. In the case under consideration, the electrical conductivity will be $\sim 10^{-5}$ and $\sim 10^{-6}$ S/cm, respectively.

The incorporation of conducting nanoparticles into the polymer medium dramatically changes its dielectric parameters, which in the alternating electric field are characterized by complex dielectric constant ε*, or permittivity

$$\varepsilon^* = \varepsilon' - i\varepsilon'', \quad (15)$$

where ε' and ε''are the real and imaginary parts of dielectric permittivity. The former value is a component of polarization that changes in phase with the alternating field, and the latter value is the contribution to polarization with the phase shifting by π/2 relative to the field and characterizes dielectric losses.

As was shown in [247], the dependence ε'(φ) may be described by the same relationship as the electrical resistance, namely, by Eq. (14): $\varphi_c = 0.006$ (0.6 wt %) and $\beta = 3.7$. The value of ε'' first increases to the critical concentration and then decreases. Equation (14a) is applicable to the growing branch of dependence ε''(φ): $\nu = 0.47$.

Metal-containing nanoparticles. It is evident that the electrophysical properties of epoxy nanocomposites with metal-containing nanoparticles depend on their conducting ability: conductor (Ag, Cu) or semiconductor (Al_2O_3, ZnO). If in the former case a filler

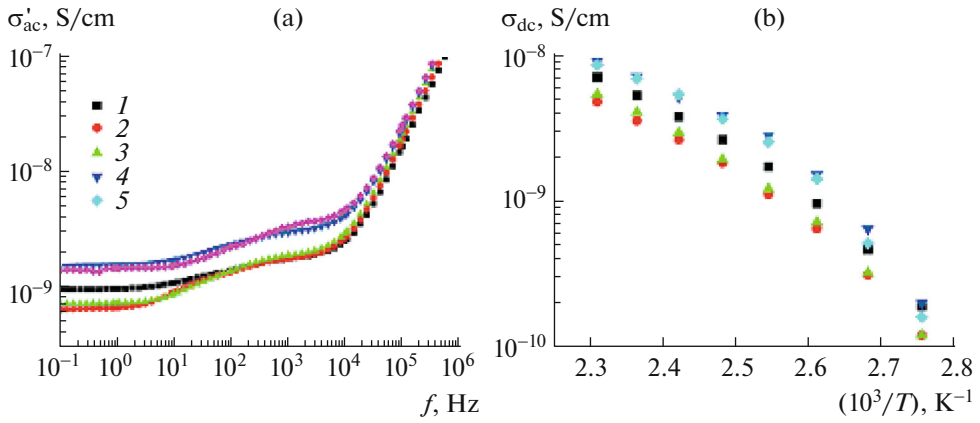

Fig. 21. (Color online) Dependences of (a) specific conductivity σ'_{ac} of the epoxy nanocomposite with ZnO on frequency at 110°C and (b) σ_{dc} of the same composite on temperature at a frequency of 1 Hz. The concentrations of ZnO nanoparticles are (*1*) 0, (*2*) 3, (*3*) 7, (*4*) 10, and (*5*) 12 wt %. The data are taken from [248].

may impart conducting properties to the composite, then in the latter case it may only modify dielectrics to a greater or lesser extent.

Semiconductors. B. Tsonos et al. [248] used dielectric relaxation spectroscopy to study epoxy nanocomposites with ZnO nanoparticles having sizes less than 100 nm. The data on specific conductivity are presented in Fig. 21.

As follows from the frequency dependence of σ'_{ac} (Fig. 21a), at low frequencies, all curves show a plateau. This corresponds to dc conductivity σ_{dc}. However, its value is small (10^{-9} S/cm). This fact implies the absence of direct current conductivity, and the applied field is compensated owing to the orientation of dipoles. Because there is no drastic difference in the curves describing the matrix and composites, it is clear that the case in point is dipoles belonging to polymer chains. Nanoparticles interacting with molecular fragments of the matrix facilitate (the concentrations of ZnO are 10 and 12%) or hinder (3 and 7%) their orientation relaxation.

The data depicted in Fig. 21b confirm this conclusion. The temperature dependence of dc conductivity is described by the empirical Vogel–Fulcher–Tammann law

$$\ln \sigma_{dc} \propto -\frac{B}{T - T_0} \qquad (16)$$

(B and T_0 are empirical constants).

This equation is usually used to describe the dynamics of relaxation of the α process in polymers. Constant T_0, which is often interpreted as a temperature of "static freezing" of electric dipoles or transition to the dipole glass state, is 30–60 K lower than T_g. Both parameters T_0 and B are related to the so-called strength parameter D via ratio $D = B/T_0$. Parameter D is inversely proportional to the value of brittleness m, which characterizes the degree of deviation from the Arrhenius dependence,

$$m = \left(\frac{\partial \log \eta}{\partial (T_g/T)}\right)_{T=T_g}, \qquad (17)$$

where η is viscosity.

The kinetic fragility index m depends on inter- and intramolecular interactions in the system and serves as a measure of bonds formed during glass transition [249].

Table 6 lists the Vogel–Fulcher–Tammann constants for the systems of interest [248, 250].

A low value of D and, accordingly, a high value of m imply that glass transition occurs in a narrow temperature range near T_g, as is typical of polymers. Thus, the fact that parameter D is almost insensitive to the existence of nanoparticles in the composite proves that the epoxy matrix makes the decisive contribution to the electrophysical properties of the epoxy nanocomposites.

The electrophysical properties of the epoxy composite with $BaTiO_3$ microparticles (smaller than 2 μm) were investigated by broadband dielectric spectroscopy [251]. It was shown that the imaginary part M'' of electric modulus M^*, which is defined as the inverse value of complex dielectric permittivity via Eq. (18), depends on the content of $BaTiO_3$ with the loss maximum monotonically decreasing with the filler concentration:

$$M^* = \varepsilon^{*-1} = (\varepsilon' - i\varepsilon'')^{-1}$$
$$= \frac{\varepsilon'}{\varepsilon'^2 + \varepsilon''^2} + i\frac{\varepsilon''}{\varepsilon'^2 + \varepsilon''^2} = M' + iM'' \qquad (18)$$

Curves $M''(f)$ exhibit peaks, which in order of increasing frequency may be assigned to interfacial polarization, also known as the Maxwell–Wagner effect; α transition (glass transition); and local β tran-

sition, which is usually attributed to the rearrangements of polar side groups of polymer chains. Figure 22 shows the temperature and concentration dependences of frequencies f_{max} corresponding to the maxima of the first two peaks.

It is seen that for all systems α transition is described by the Vogel–Fulcher–Tammann equation, whereas interfacial polarization obeys the Arrhenius law. The energy of activation for the process of interfacial polarization somewhat increases with the content of $BaTiO_3$, but in both cases the dependence on the filler concentration is very weak. Note that interfacial polarization almost always occurs in polymers owing to the presence of various additives, plasticizers, etc. Parameter T_0 also increases with the filler content according to a rise in the glass-transition temperature.

Hence, the patterns of the temperature and frequency dependence M'' of the composites confirm that the epoxy matrix makes the decisive contribution to the electrophysical properties of the epoxy nanocomposites.

S. Singha and M.T. Thomas [252] compared the epoxy nanocomposites with TiO_2, Al_2O_3, and ZnO nanoparticles as insulators. The highest efficiency was exhibited by TiO_2, which decreased the dc resistance of the matrix from 7×10^{17} to $\sim 2 \times 10^{17}$ Ω cm for the composite containing 0.5 wt % TiO_2. Then follow ZnO ($\sim 3 \times 10^{17}$ Ω cm, a concentration of 0.5 wt %) and, finally, Al_2O_3 ($\sim 4 \times 10^{17}$ Ω cm, a concentration of 5 wt %). The effect of the filler type on the specific dc resistance of nanocomposites is not very high. Probably, this phenomenon may be explained by the fact that excess free charges are introduced in the composite by particles. The phenomenon is the most pronounced in the case of TiO_2.

An analogous effect is exhibited by these fillers on the ac dielectric strength. The probability of breakdown was analyzed in terms of the Wiebull distribution

$$F(x) = 1 - \exp\{-(x/\lambda)^{\beta}\} \quad (19)$$

(λ is the scale parameter, and β is the shape parameter).

The presence of nanoparticles increases the probability of breakdown via a marked reduction in the value of λ. For example, λ is 28.6 kV/mm at 0.5% ZnO, whereas for the matrix λ = 52.3. In the case of Al_2O_3, the scale parameter is 36–40 kV/mm.

Figure 23 plots the ac dielectric strength of the epoxy nanocomposites as a function of the concentration and size of ZnO particles [253]. If at low concentrations (less than 10%) the size of nanoparticles has almost no effect, then at a high filling (above 10%) coarse particles (~500 nm) decrease the electric strength much more strongly than fine particles (~65 nm).

Table 6. Vogel–Fulcher–Tammann constants for the epoxy nanocomposites with ZnO

Content of ZnO, %	B, K	T_0, K	D
0	714/754	268/263	2.7/2.9
2.9	600/700	279/268	2.2/2.6
4.8	–/675	–/271	–/2.5
6.5	699/611	274/274	2.6/2.3
9.1	712/608	274/278	2.6/2.2
10.7	612/550	276/281	2.2/2.0

The data taken from [248] are in the numerator, and the data taken from [250] are in the denominator.

Q. Wang and G. Chen demonstrated [254] that the ac dielectric strength of epoxy nanocomposites is considerably affected not only by the type of the filler but also by the interfacial layer. For example, the treatment of SiO_2 nanoparticles with silane leads to an increase in λ from 140.1 (matrix) to 151.4 kV/mm, whereas for the untreated particles λ = 130.5 kV/mm.

The interfacial layer plays an important role in controlling the properties of composites. However, at a low concentration of nanoparticles, its contribution can hardly be determined. Using broadband dielectric spectroscopy, X. Huang et al. [255] studied highly filled epoxy nanocomposites containing 50 vol % $BaTiO_3$ nanoparticles with six kinds of surface chemistry (Fig. 24). It was assumed that in this case exactly interfacial layers would exert the decisive effect on the properties of the composite.

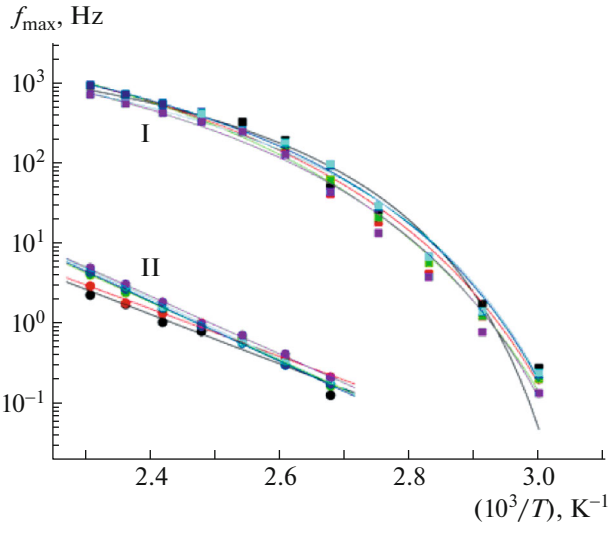

Fig. 22. (Color online) Temperature and concentration dependences of f_{max} corresponding to (I) the α transition and (II) the interfacial polarization effect. The concentration of $BaTiO_3$ is varied from 0 to 13.6 vol %. The data are taken from [251].

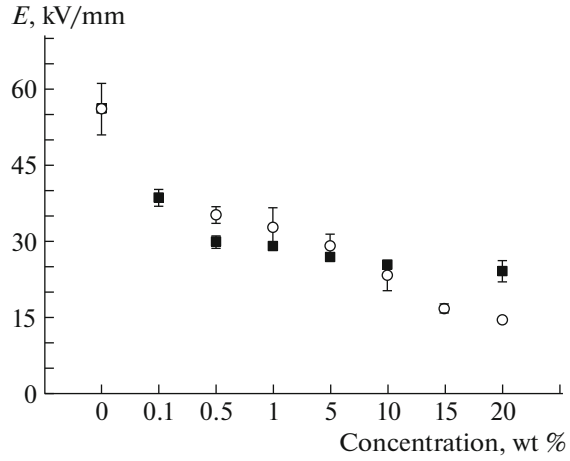

Fig. 23. Dependence of the ac dielectric strength of the epoxy nanocomposite on the concentration of ZnO particles with a size of 65 (closed circles) and 500 nm (open circles). The data are taken from [253].

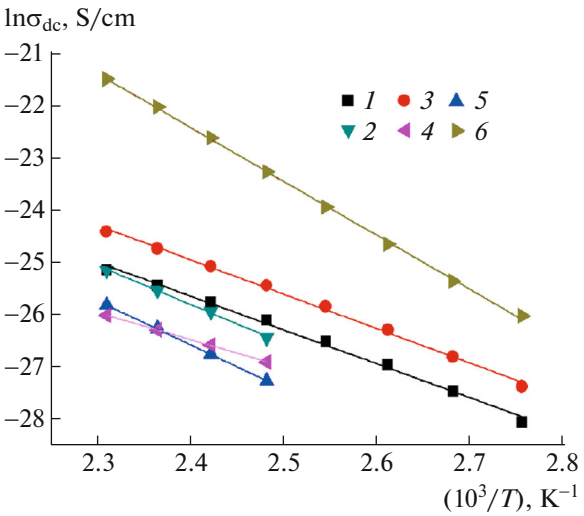

Fig. 24. (Color online) Temperature dependence of the dc conductivity of the epoxy nanocomposite with $BaTiO_3$ nanoparticles (*1*) without treatment and with (*2*) SH, (*3*) OH, (*4*) NH_2, and (*5*) epoxy grafted groups and (*6*) hyperbranched aromatic polyamide. The data are taken from [255].

As opposed to the dependence plotted, for example, in Fig. 22, the Arrhenius law holds in this case. This implies that the matrix does not make itself evident. The energy of activation E_a of conduction depends on the chemical nature of groups grafted onto the surface of nanoparticles, i.e., on the structure of the interfacial layer. The lowest values of E_a are exhibited by structures formed using amino and epoxy groups able to directly participate in formation of the matrix network (straight lines *3*, *4*). This is apparently the densest layer. The mobility of polymer chains is restricted, and the dipole or orientation contribution to polarizability will be minimal. The most mobile molecular fragment providing a high conductivity is the layer obtained with participation of the hyperbranched aromatic polyamide. The same layer exhibits the highest activation energy (straight line *6*).

Conductors. Among conducting metal nanoparticles, silver is distinguished by its excellent electrical conductivity. In [256], epoxy nanocomposites were obtained using a powder Ag with a size of 70 nm. Direct measurements demonstrated that the dc conductivity is described by relationship (14) at $\varphi_c = 1 \pm 0.3\%$ and $\beta = 5 \pm 0.5$. Usually $\varphi_c = 15\%$ and $\beta = 2$ [257]. The authors attributed this discrepancy to the aggregation of nanoparticles into chain structures with a high aspect ratio; therefore, the percolation threshold decreases. Another possible reason may be the enlargement of nanoparticles, but as shown in [257] (really, for microparticles), this leads to a reduction in φ_c.

At the same time, ac measurements performed in [256] are in conflict with the above data. Figure 25 presents the data on the ac conductivity. As in the case of multiwall CNTs (Fig. 20), at low frequencies and fairly high concentrations of Ag nanoparticles, curves $\sigma_{ac}(f)$ cease to be frequency dependent, thereby demonstrating the transition to σ_{dc}. However, it is seen that, at concentrations of 2.2 and 3.3%, there is no any sign of such a tendency. A sharp attainment of the plateau corresponds to 8.3%. Hence, $\varphi_c \geqslant 1\%$.

Using powder Ag with a size of 200 nm as a filler, S. Nam et al. [258] showed that, in accordance with electrical resistance measurements, the percolation threshold is nearly 0.23. Interestingly, the addition of SiO_2 microparticles (1–5 μm) in an amount of 12 vol % shifts the threshold to ~0.18. On the basis of electron microscopy studies, the authors believe that the supramolecular structure of the matrix becomes more uniform upon introduction of the additives.

Further studies [259] showed that the size of SiO_2 particles is of great importance. When 5 vol % nanoparticles with a diameter of 1000 nm was added, the percolation threshold φ_c was reduced from 0.23 to 0.14. Eventually, nanoparticles with a smaller diameter (500, 80, and 10 nm) decreased φ_c to 0.1.

In [145], silver nanoparticles with a size of 15–20 nm were synthesized in situ via the reduction of $AgSbF_6$. The percolation threshold according to the ac conductivity measurements was not reached even at 20 wt % precursor; this value corresponded to approximately 5 wt % or ~0.5 vol % Ag nanoparticles, which is quite natural.

At filler concentrations not above φ_c, dielectric spectroscopy measurements reflect relaxation properties of the matrix and the influence of nanoparticles on them. For example, as was shown in [146], which is a

continuation of the previous study, the dependence of complex dielectric permittivity ε^* on frequency ω is described by the Havriliak–Negami equation

$$\varepsilon^*(\omega) = \varepsilon_\infty + \frac{\varepsilon_0 - \varepsilon_\infty}{[1 + (i\omega\tau)^\alpha]^\beta}, \quad (20)$$

where ε_∞ and ε_0 are the dielectric permittivity at ultimately high and low frequencies, τ is the time of relaxation, and α and β are the parameters generalizing various types of relaxation: $\alpha = \beta = 1$ (the Debye equation), $\alpha = 0$ and $\beta \neq 0$ (the Cole–Davidson equation), and $\alpha \neq 0$ and $\beta = 0$ (the Cole–Cole equation).

In the presence of Ag nanoparticles, low-temperature peaks on the curves $\varepsilon''(\omega)$ corresponding to the β relaxation shift to high frequencies, which, most probably, characterizes the effect of plasticization. The same argument may be used to explain reduction in the energy of activation from 61 (matrix) to 50 kJ/mol (4.1 wt % Ag) in the Arrhenius dependence $\tau(T)$.

Peaks on the curves of the imaginary part M'' of electric modulus M^* which refer to the interfacial polarization also shift to high frequencies with an increase in the concentration of Ag, and the energies of activation, as calculated from the temperature dependence of their frequency, grow to 159 kJ/mol, thereby demonstrating an increase in the heterogeneity of the system.

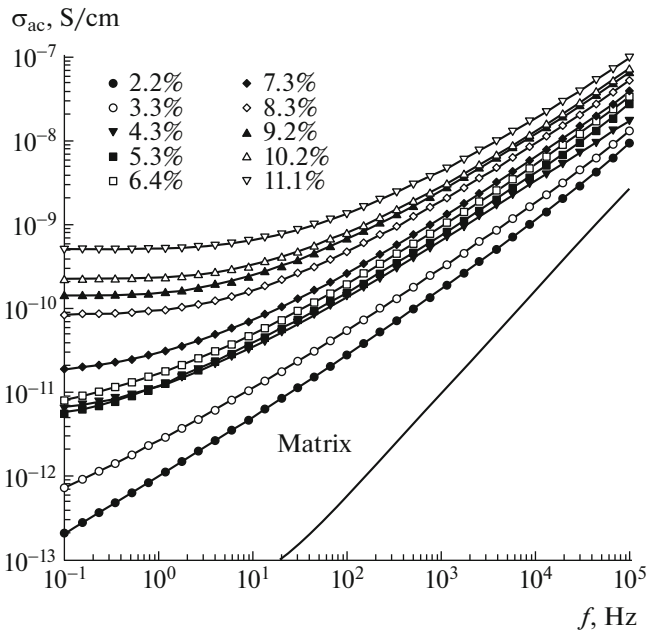

Fig. 25. Frequency and concentration dependences of the ac conductivity of the epoxy nanocomposite with silver nanoparticles. The data are taken from [256].

Magnetic Properties

It is evident that the magnetic properties of the epoxy nanocomposites are determined by nanoparticles possessing a magnetic moment. Specifically, magnetite Fe_3O_4 features a high saturation magnetization ($M_c \sim 92$–100 emu/g at room temperature). Therefore, upon incorporation into the polymer matrix, magnetite may be extensively used in such applications as magnetic resonance tomography, biomedical sensors, screening of electromagnetic disturbances, flexible electronics, magneto-optical storage devices, etc. However, because surface functional groups able to react with the epoxy matrix are in deficiency, Fe_3O_4 nanoparticles are easily involved in agglomeration because of a strong magnetic dipole–dipole interaction between particles.

In [260], magnetic epoxy nanocomposites were prepared. The functionalization of Fe_3O_4 nanoparticles by polyaniline was implemented via surface-initiated polymerization.

The experiments showed that, in the epoxy nanocomposites containing 15 wt % of both functionalized and nonfunctionalized nanoparticles at room temperature, there was no loop of magnetic hysteresis. Its absence on all magnetization curves with an almost zero coercivity indicates the superparamagnetic behavior of the composites. This is apparently associated with the fact that the sizes of magnetite nanoparticles are below the critical value (10–20 nm), so that every particle may serve as one magnetic domain with a high permanent magnetic moment and may behave as a huge paramagnetic atom. This nanoparticle may rapidly respond to the applied magnetic field with a small coercivity and an insignificant residual magnetization.

For all of the samples, saturation magnetization M_c was not attained even under application of a strong magnetic field H. This parameter was estimated by extrapolating dependence $M_c(H^{-1})$. The as-calculated values of M_c for nanoparticles were much lower than those for bulk Fe_3O_4 samples: the level of magnetization for the 15% epoxy nanocomposite was about 9.5 emu/g.

Jacobsite $MnFe_2O_4$, whose nanoparticles were used to prepare magnetic epoxy nanocomposites [261], exhibits ferromagnetic behavior, being a magnetite. Table 7 lists the magnetic characteristics of the composite in comparison with the crystalline $MnFe_2O_4$: coercivity H_c, saturation magnetization M_c, and magnetic moment m.

The growth of coercivity and magnetic moments for the nanocomposites may be associated with the presence of hydrogen bonds in the epoxy matrix. The magnetization of a composite is governed by dimensionality of the network of hydrogen bonds with their coordinated movement playing the role of exchanging paths between magnetic centers and causing their remagnetization [262].

The value of M_c is affected by the dipole interaction of nanoparticles, which grows with the concentration

Table 7. Magnetic properties of epoxy nanocomposites with $MnFe_2O_4$ [261]

System	H_c, Oe	M_c, emu/g	m, μ_B
Neat $MnFe_2O_4$	14.9	31.68	1.244
5% epoxy nanocomposite	44.7	1.84	1.373
10% epoxy nanocomposite	43.9	4.21	1.354

of the filler. It appears that this finding may provide an explanation for the data summarized in Table 7.

This dependence is confirmed by the data on the magnetic properties of epoxy nanocomposites containing inclusions of barium ferrite $BaFe_{12}O_{19}$ nanoparticles [263] (Fig. 26). As is clear, not only the saturation magnetization (straight line *1*) but also the residual magnetization (straight line *2*) linearly increase with the concentration of $BaFe_{12}O_{19}$. The limiting values of the mentioned parameters are 14.0 and 4.1 emu/g, respectively. Note that the coercivity is the same for all of the systems: H_c = 1.3 kOe.

In order to impart magnetic properties to epoxy nanocomposites, X. Zhang et al. [284] used graphene with the deposited product of thermal decomposition of $Fe(CO)_5$—a mixture of Fe and Fe_2O_3. The saturation magnetization of the composite was 0.04, 0.16, and 0.45 emu/g for 1.0, 3.0, and 5.0 wt %, respectively. For the neat filler, M_c was 14.7 emu/g. Hence, the calculated values of M_c for the same concentrations should be 0.15, 0.44, and 0.74 emu/g. In the author's opinion, reduction in M_c for the nanoparticles may be attributed to the oxidation of iron during the curing process.

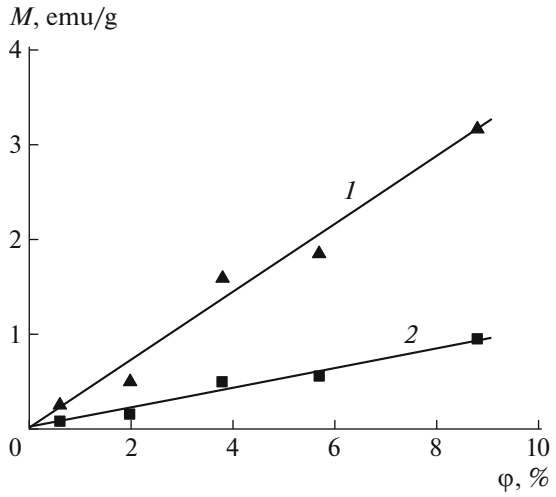

Fig. 26. Dependence of (*1*) saturation magnetization and (*2*) residual magnetization on the volume fraction of the $BaFe_{12}O_{19}$ filler. The data are taken from [263].

The coercivity is inversely proportional to the filler content: 67.2, 46.5, and 12.3 Oe, respectively.

In order to protect iron (and other variable valence metals) from further oxidation, nanoparticles with the core–shell structure are employed and noble metals, carbon, and oxides of iron are used as a shell [265]. The latter metal was used in [266]: Fe (core) + FeO (shell) with a particle size of 15–25 nm and an oxide thickness of 0.5 nm.

As in previous cases, the saturation magnetization grows with the concentration of nanoparticles. M_c = 17 emu/g for the epoxy nanocomposites with 20 wt % nanoparticles. This value is ~16% from the corresponding value of the block filler. During dispersion, the coercivity grows from 62.33 to 202.13 Oe. This observation may be explained by weakening of interparticle dipole interaction because of an increased distance between single-domain nanoparticles compared with nanoparticles that are in close contact in the block.

A change of the shell of nanoparticles from FeO to the carbon one [267] leads to reduction in the saturation magnetization and causes a rise in coercivity. This tendency may also be explained by the worsening of interparticle dipole interaction.

Thermal Conductivity of Epoxy Nanocomposites

Thermal conductivity is closely related to electrical conductivity. For example, in metals, according to the Wiedemann–Franz law, the thermal conductivity coefficient K is directly proportional to electrical conductivity. However, carbon fillers featuring an extremely high thermal conductivity and a low specific gravity do not demonstrate the expected improvement of thermal conductivity in epoxy nanocomposites largely because of their poor dispersion and problems related to the nature of interfacial layers, in particular, to the Kapitza thermal resistance R_k.

Figure 27 shows the concentration dependences of the thermal conductivity coefficient K for the epoxy nanocomposites with a number of carbon nanofillers [268]. The best results are obtained for graphene flakes (curve *1*), i.e., growth by a factor of ~10 at 10 wt % multiwall CNTs. At the same concentration (curve *2*), the thermal conductivity of the matrix increases by approximately five times. But in this case, the electrical conductivity grows by five to seven orders of magnitude. Nevertheless, proportionality between these values (K and σ_{dc}) is preserved if the percolation threshold of multiwall CNTs is overcome [269]. The same relationship is observed between K and σ_{ac} at lower concentrations of graphene that was obtained by the sonification exfoliation of graphite oxide [270].

An important role of the interfacial layer was demonstrated by C.-C. Teng et al. [271], who used poly(glycidyl methacrylate) with the terminal pyrene group for the noncovalent functionalization of

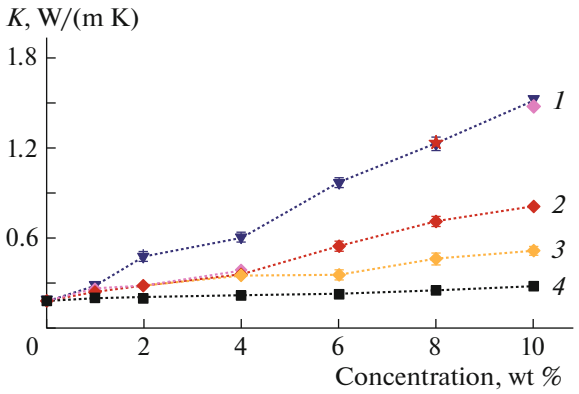

Fig. 27. (Color online) The concentration dependence of thermal conductivity K of epoxy nanocomposites with fillers: (*1*) graphene, (*2*) multiwall CNTs, (*3*) graphene oxide, and (*4*) graphite. The data are taken from [268].

graphene. The thermal conductivity of the epoxy nanocomposites containing ~4 wt % of these nanoparticles was 1.91 W/(m K), which is ~20% higher than that in the case of nonfunctionalized graphene.

The thermal resistance of the boundary layer, which is known as the Kapitza thermal resistance, is $R_k \approx 8 \times 10^{-8}$ m^2/(K W). This value refers not only to CNTs and other carbon fillers of epoxy matrices but also to other composite materials and polycrystals [272]. Even a slight increase in R_k entails a marked worsening of the thermal conductivity of the composite, despite high values of the thermal conductivity coefficient and the aspect ratio of nanoparticles. As was revealed by molecular dynamics modeling performed using SiC nanoparticles, taking into account contributions of the Kapitza resistance and the effective interfacial layer to the overall thermal conductivity is a general and important analytical consideration in analysis of the thermal properties of epoxy nanocomposites, in particular, the effect of dependence on the size of particles [273].

In accordance with [274], for nanoparticles with a small aspect ratio at volume fraction $\varphi \geq \varphi_c$ the percolation theory gives

$$\ln\left(\frac{\lambda}{\lambda_f}\right) = \left(\frac{1-\varphi}{1-\varphi_c}\right)^n \times \ln\left(\frac{\lambda_c}{\lambda_f}\right) \quad (21)$$

Here λ, λ_f, and λ_c are the thermal conductivities of a composite, of a filler, and at the percolation concentration φ_c. Exponent n depends on the size and shape of the filler and the character of its distribution in a composite.

Because a marked gain in the thermal conductivity of polymer composites is feasible only above the percolation threshold, the use of metal nanoparticles for this purpose presents a problem. In fact, for particles with the aspect ratio on the order of unity, $\varphi_c \sim 0.15$; that is, the weight fraction of the metal filler is extremely high. An example is provided by paper [275], in which K was 27 W/(m K) at a volume content of silver nanoparticles of 45%, which corresponds to their weight concentration of 86%.

CONCLUSIONS

It has been shown that, regardless of whether a filler is introduced in the reaction system or is formed in situ during the process of matrix formation, its structure changes to a greater or lesser extent compared with the unfilled cured epoxy binder. In addition, the matrix influences the character of distribution of nanoparticles over volume. This effect is especially important in the case of graphene and MMT, when exfoliation is the case in point. The matrix governs the size and shape of the resulting nanoparticles. Their interaction with the epoxy resin affords interfacial layers. There is no doubt that all these factors affect the properties of the epoxy nanocomposites.

The application areas of composites are defined by both the physicomechanical parameters of the epoxy matrix, its strength, thermomechanical stability, and adhesion ability and the unique properties of nanoparticles.

Nanoparticles of gold, silver, copper, TiO_2, ZnO, fullerene, and CNTs demonstrate effective antibacterial properties; therefore, composites containing these nanoparticles may be used for the microbiological control and purification of water, disinfection of surfaces, and creation of germicidal coatings, protective films, etc. Silver shows anti-inflammatory behavior and features antiviral and antifungal abilities. Its application in the form of nanoparticles (compared with the ionic form) decreases the cellular toxicity rather than the antibacterial efficiency [276, 277].

Dielectric and magnetic polymer nanocomposites have found wide use in such fields as Fourier spectroscopy, NMR, data storage, and absorption of electromagnetic radiation from other objects. Epoxy nanocomposites are not exception. The role of nanoparticles shows itself as improvement of electric strength and stress durability, suppression of space charge, and increase in the stability of dielectric discharge. For example, in the case of built-in planar capacitors, the insertion of dielectric films between copper sheets makes it possible to efficiently reduce the number of assembly devices. This not only leads to the miniaturization of circuit boards and electric wiring but also improves the characteristics of devices (e.g., promotes reduction in electromagnetic interference and switching noises) [255, 261, 263].

Epoxy resins are often employed in antiwear applications. The use of such fillers as graphene oxide [278] or complexes MMT + SiO_2 [229] and cloisite + TiO_2 [279], even at their very low content, decreases the rate of material wear by almost an order of magnitude.

The present review covers far from all aspects of the processes of formation, properties, and application of epoxy nanocomposites which deserve consideration. We did not go into the details of kinetics and mechanisms of chemical reactions of epoxy oligomers, assuming that these issues have sufficiently been highlighted in the literature [40, 41, 280].

Evidently, little attention has been paid to relaxation properties. Problems pertaining to thermal stability and heat resistance are beyond the scope of this review. One of the reasons is the ambiguity of the published data.

As for the application of epoxy nanocomposites, in our opinion, this subject deserves a separate article.

In conclusion, it should be noted that, although many papers devoted to various problems of epoxy nanocomposites have been published in recent years, these fields of science and engineering are progressing so rapidly that after two to three years the need for a new generalization will arise.

REFERENCES

1. A. D. Pomogailo and G. I. Dzhardimalieva, *Metal-Polymer Hybrid Nanocomposites* (Nauka, Moscow, 2015) [in Russian].
2. *Polymer Nanocomposites,* Ed. by Y.-W. Mai and Z.-Z. Yu (Cambridge, Woodhead, 2006).
3. A. I. Gusev, *Nanomaterials, Nanostructures, Nanotechnologies* (Fizmatlit, Moscow, 2007) [in Russian].
4. I. P. Suzdalev, *Nanotechnology. Physics and Chemistry of Nnaocrystals, Nanostructures and Nanomaterials* (Kom Kniga, Moscow, 2006) [in Russian].
5. A. D. Pomogailo, A. S. Rozenberg, and I. E. Uflyand, *Metal Nanoparticles in Polymers* (Khimiya, Moscow, 2000) [in Russian].
6. A. D. Pomogailo and G. I. Dzhardimalieva, *Nanostructured Materials Preparation via Condensation Ways* (Springer Sci.+Business Media, Dordrecht, 2014).
7. *Advances in Diverse Industrial Applications of Nanocomposites,* Ed. by B. Reddy (InTech, Rijeka, Croatia, 2011).
8. *Advances in Nanocomposites – Synthesis, Characterization and Industrial Applications,* Ed. by B. Reddy (InTech, Rijeka, Croatia, 2011).
9. *Optimization of Polymer Nanocomposite Properties,* Ed. by V. Mittal (Wiley-VCH Verlag, Weinheim, 2010).
10. B. Sarkar and P. Alexandridis, Prog. Polym.Sci **40**, 33 (2015).
11. P. Rao, P. Gruenberg, and K. E. Geckeler, Prog. Polym. Sci. **40**, 138 (2015).
12. G. V. Kozlov, Phys.-Usp. **58** (1), 33 (2015).
13. Y. G. Jeong and J.-E. An, Polym. Int. **63** (11), 1895 (2014).
14. H. Li, J. V. John, S. J. Byeon, M. S. Heo, J. H. Sung, K.-H. Kim, and I. Kim, Prog. Polym. Sci. **39**, 1878 (2014).
15. V. A. Gerasin, E. M. Antipov, V. V. Karbushev, V. G. Kulichikhin, G. P. Karpacheva, R. V. Talroze, and Y. V. Kudryavtsev, Russ. Chem. Rev. **82** (4), 303 (2013).
16. S. H. Song, K. H. Park, B. H. Kim, Y. W. Choi, G. H. Jun, D. J. Lee, B.-S. Kong, K.-W. Paik, and S. Jeo, Adv. Mater. **25** (5), 732 (2013).
17. I. V. Gmoshinski, S. A. Khotimchenko, V. O. Popov, B. B. Dzantiev, A. V. Zherdev, V. F. Demin, and Yu. P. Buzulukov, Russ. Chem. Rev. **82** (1), 48 (2013).
18. V. P. Smagin, Obz. Zh. Khim. **3** (1), 180 (2013).
19. E. N. Kablov and S. V. Kondrashov, and G. Yu. Yurkov, Nanotechnol. Russ. **8** (3), 163 (2013).
20. D. Kim, S. Srivastava, S. Narayanan, and L. A. Archer, Soft Matter **8** (42), 10813 (2012).
21. Y. Du, S. Z. Shenb, K. Caia, and P. S. Casey, Prog. Polym. Sci. **37** (6), 830 (2012).
22. V. I. Irzhak, Russ. Chem. Rev. **80** (8), 787 (2013).
23. M. Terrones, O. Martín, M. González, J. Pozuelo, B. Serrano, J. C. Cabanelas, S. M. Vega-Díaz, and J. Baselga, Adv. Mater. **23** (44), 5302 (2011).
24. J. R. Potts, D. R. Dreyer, C. W. Bielawski, and R. S. Ruoff, Polymer **52** (1), 5 (2011).
25. Z. Han and A. Fina, Prog. Polym. Sci. **36** (7), 914 (2011).
26. K. Haraguchi, Polym. J. **43** (3), 223 (2011).
27. V. Singh, D. Joung, L. Zhai, S. Das, S. I. Khondaker, and S. Seal, Prog. Mater. Sci. **56** (8), 1178 (2011).
28. A. Yu. Olenin and G. V. Lisichkin, Russ. Chem. Rev. **80** (7), 605 (2011).
29. T. Kuilla, S. Bhadra, D. Yao, N. H. Kim, S. Bose, and J. H. Lee, Prog. Polym. Sci. **35** (11), 1350 (2010).
30. E. R. Badamshina, M. P. Gafurova, and Ya. I. Estrin, Russ. Chem. Rev. **79** (11), 945 (2010).
31. S. K. Kumar and R. Krishnamoorti, Annu. Rev. Chem. Biomol. Eng. **1**, 37 (2010).
32. M. A. Tasdelen, J. Kreutzer, and Y. Yagci, Macromol. Chem. Phys. **211** (3), 279 (2010).
33. Z. Spitalsky, D. Tasis, K. Papagelis, and C. Galiotis, Prog. Polym. Sci. **35** (3), 357 (2010).
34. N. G. Sahoo, S. Rana, J. W. Cho, L. Li, and S. H. Chan, Prog. Polym. Sci. **35** (7), 837 (2010).
35. A. M. Paquin, *Epoxydverbindungen und Epoxydharze* (Springer, Berlin, 1958).
36. H. Lee and K. Neville, *Handbook of Epoxy Resins* (McGraw-Hill, New York, 1967).
37. I. Z. Chernin, F. M. Smekhov, and Yu. V. Zherdev, *Epoxy Polymers and Compositions* (Khimiya, Moscow, 1982) [in Russian].
38. V. G. Khozin, *Reinforcement of Epoxy Polymers* (Dom pechati, Kazan, 2004) [in Russian].
39. V. I. Irzhak, B. A. Rozenberg, and N. S. Enikolopyan, *Crosslinked Polymers. Synthesis, Structure, Properties* (Nauka, Moscow, 1979) [in Russian].
40. B. A. Rozenberg, Adv. Polym. Sci. **75**, 113 (1986).
41. T. Okabe, T. Takehara, K. Inose, N. Hirano, M. Nishikawa, and T. Uehara, Polymer **54** (17), 4660 (2013).
42. K. E. Perepelkin, *Reinforcing Fibers and Fibrous Polymer Composites* (Nauchnye osnovy i tekhnologii, Moscow, 2009) [in Russian].

43. E. S. Zelenskii, A. M. Kuperman, Yu. A. Gorbatkina, V. G. Ivanova-Mumzhieva, and A. A. Berlin, Ross. Khim. Zh. **45** (1), 56 (2001).
44. P. N. D'yachkov, *Carbon Nanotubes. Structure, Properties, Application* (Binom, Moscow, 2006) [in Russian].
45. E. G. Rakov, *Nanotubes and Fullerenes* (Universitetskaya kniga, Moscow, 2006) [in Russian].
46. E. G. Rakov, Russ. Chem. Rev. **82** (1), 27 (2013).
47. A. L. Ivanovskii, Russ. Chem. Rev. **81** (7), 571 (2012).
48. E. D. Grayfer, V. G. Makotchenko, A. S. Nazarov, S. J. Kim, and V. E. Fedorov, Russ. Chem. Rev. **80** (8), 751 (2011).
49. A. Schaetz, M. Zeltner and W. J. Stark, ACS Catal. **2** (6), 1267 (2012).
50. S. Navalon, A. Dhakshinamoorthy, M. Alvaro, and H. Garcia, Chem. Rev. **114** (12), 6179 (2014).
51. C. K. Chua and M. Pumera, Chem.-Eur. J. **21** (36), 12550 (2015).
52. D. A. Britz and A. N. Khlobystov, Chem. Soc. Rev. **35** (7), 637 (2006).
53. B. Xue, J. Zhu, N. Liu, and Y. Li, Catal. Commun. **64**, 105 (2015).
54. B. Shen, W. Zhai, M. Tao, D. Lu, and W. Zheng, Compos. Sci. Technol. **77**, 87 (2013).
55. Z. Liang, J. Gou, C. Zhang, B. Wang, and L. Kramer, Mater. Sci. Eng., A **365** (1–2), 228 (2004).
56. H. Xie, B. Liu, Z. Yuan, J. Shen, and R. Cheng, J. Polym. Sci., Part A: Polym. Chem. **42** (20), 3701 (2004).
57. K. Tao, S. Yang, J. C. Grunlan, Y.-S. Kim, B. Dang, Y. Deng, R. L. Thomas, B. L. Wilson, and X. Wei, J. Appl. Polym. Sci. **102** (6), 5248 (2006).
58. E. Esmizadeh, A. A. Yousefi, and G. Naderi, Iran Polym. J. **24** (1), 1 (2015).
59. A. Visco, L. Calabrese, and C. Milone, J. Reinf. Plast. Compos. **28** (8), 937.
60. S. B. Susin, V. Pistor, S. C. Amico, L. A. F. Coelho, S. H. Pezzin, and A. J. Zattera, J. Appl. Polym. Sci. **131** (3), 39857 (2014).
61. A. Rahaman and A. Mohanty, Polym. Compos. **35** (29), 441 (2014).
62. S. Vyazovkin and N. Sbirrzaauoli, Macromolecules **29** (6), 1867 (1996).
63. L. S. Cividanes, E. A. N. Simonetti, M. B. Moraes, F. W. Fernandes, and G. P. Thim, Polym. Eng. Sci. **54** (11), 2461 (2014).
64. T. Zhou, X. Wang, and T. Wang, Polym. Int. **58** (4), 445 (2009).
65. M. Abdalla, D. Dean, P. Robinson, and E. Nyairo, Polymer **49** (16), 3310 (2008).
66. L. Valentini, D. Puglia, F. Carniato, E. Boccaleri, L. Marchese, and J. M. Kenny, Compos. Sci. Technol **68** (3–4), 1008 (2008).
67. J. Qiu and S. Wang, Mater. Chem. Phys. **121** (1–2), 295 (2010).
68. W. J. Choi, R. L. Powell, and D. S. Kim, Polym. Compos. **30** (4), 415 (2009).
69. K. Yang, M. Gu, Y. Jin, G. Mu, and X. Pan, Composites, Part A **39** (10), 1670 (2008).
70. L. S. Cividanes, D. D. Brunelli, E. F. Antunes, E. J. Corat, K. K. Sakane, and G. P. Thim, J. Appl. Polym. Sci. **127** (1), 544 (2013).
71. S. V. Kondrashov, V. P. Grachev, R. V. Akatenkov, V. N. Aleksashin, I. S. Deev, I. V. Anoshkin, E. G. Rakov, and V. I. Irzhak, Polym. Sci., Ser. A **56** (3), 330 (2014).
72. S. L. Qiu, C. S. Wang, Y. T. Wang, C. G. Liu, X. Y. Chen, H. F. Xie, Y. A. Huang, and R. S. Cheng, eXPRESS Polym. Lett. **5** (9), 809 (2011).
73. S. H. Ryu, J. H. Sin, and A. M. Shanmugharaj, Eur. Polym. J. **52**, 88 (2014).
74. J. K. Park and D. S. Kim, Polym. Eng. Sci. **54** (4), 969 (2014).
75. J. K. Park and D. S. Kim, Polym. Eng. Sci. **54** (5), 985 (2014).
76. D. G. D. Galpaya, J. F. S. Fernando, L. Rintoul, N. Motta, E. R. Waclawik, C. Yan, and G. A. George, Polymer **71**, 122 (2015).
77. M. R. Acocella, C. E. Corcione, A. Giuri, M. Maggio, A. Maffezzoli, and G. Guerra, RSC Adv. **6** (28), 23858 (2016).
78. M. Mauro, M. R. Acocella, C. E. Corcione, A. Maffezzoli, and G. Guerra, Polymer **55**, 5612 (2014).
79. L. Li, Z. Zeng, H. Zou, and M. Liang, Thermochim. Acta **614**, 76 (2015).
80. A. T. Seyhan, Z. Sun, J. Deitzel, M. Tanoglu, and D. Heider, Mater. Chem. Phys. **118** (1), 234 (2009).
81. Z.-Q. Cai, S. Movva, N.-R. Chiou, D. Guerra, Y. Hioe, J. M. Castro, and L. J. Lee, J. Appl. Polym. Sci. **118** (4), 2328 (2010).
82. R. Sanctuary, J. Baller, B. Zielinski, N. Becker, J. K. Krüger, U. Philipp, M. Müller, and M. Ziehmer, J. Phys.: Condens. Matter **21** (3), 035118 (2009).
83. J. Baller, M. Thomassey, M. Ziehmer, and R. Sanctuary, Thermochim. Acta **517** (1–2), 34 (2011).
84. E. N. Karasinski, M. G. D. Luz, C. M. Lepienski, and L. A. F. Coelho, Thermochim. Acta **569**, 167 (2013).
85. O. Zabihi, S. M. Mostafavi, F. Ravari, A. Khodabandeh, A. Hooshafza, K. Zare, and M. Shahizadeh, Thermochim. Acta **521** (1–2), 49 (2011).
86. M. Ghaffari, M. Ehsani, M. Vandalvand, E. Avazverdi, A. Askari, and A. Goudarzi, Prog. Org. Coat **89**, 277 (2015).
87. O. Zabihi, A. Hooshafza, F. Moztarzadeh, H. Payravand, A. Afshar, and R. Alizadeh, Thermochim. Acta **527**, 190 (2012).
88. A. Omrani, A. A. Rostami, F. Ravari, and A. Mashak, Thermochim. Acta **517** (1–2), 9 (2011).
89. S. G. Hong and J. S. Tsai, J. Therm. Anal. Calorim. **63** (1), 31 (2001).
90. J. Baller, N. Becker, M. Ziehmer, M. Thomassey, B. Zielinski, U. Müller, and R. Sanctuary, Polymer **50** (14), 3211 (2009).
91. P. Rosso and L. Ye, Macromol. Rapid Commun. **28** (1), 121 (2007).
92. M. Ghaemy, S. M. Amini Nasab, and M. Barghamadi, J. Appl. Polym. Sci. **104** (6), 3855 (2007).

93. C. Alzina, N. Sbirrazzuoli, and A. Mija, J. Phys. Chem. C **115** (46), 22789.
94. S. Pavlidou and C. D. Papaspyrides, Prog. Polym. Sci. **33** (12), 1119 (2008).
95. O. Becker and G. P. Simon, Adv. Polym. Sci. **179**, 29 (2005).
96. L. B. Paiva, A. R. de Morales, and F. R. Valenzuela Diaz, Appl. Clay Sci. **42** (1–2), 8 (2008).
97. C. Alzina, A. Mija, L. Vincent, and N. Sbirrazzuoli, J. Phys. Chem. B **116** (19), 5786.
98. M. Ivankovic, I. Brnardic, H. Ivankovic, and H. J. Mencer, J. Appl. Polym. Sci. **99** (2), 550 (2006).
99. C. Alzina, N. Sbirrazzuoli, and A. Mija, J. Phys. Chem. B **114** (39), 12480.
100. F. Román, Y. Calventus, P. Colomer, and J. M. Hutchinson, Thermochim. Acta **541**, 76 (2012).
101. L. Li, H. Zou, M. Liang, and Y. Chen, Thermochim. Acta **597**, 93 (2014).
102. F. Ferdosian, M. Ebrahimi, and A. Jannesari, Thermochim. Acta **568**, 67 (2013).
103. A. M. Shanmugharaj and S. H. Ryu, Thermochim. Acta **546**, 16 (2012).
104. F. Shiravand, J. M. Hutchinson, and Y. Calventus, Polym. Eng. Sci. **54** (1), 51 (2014).
105. S. Montserrat, F. Román, J. M. Hutchinson, and L. Campos, J. Appl. Polym. Sci. **108** (2), 923 (2008).
106. P. Cortés, I. Fraga, Y. Calventus, F. Román, J. M. Hutchinson, and F. Ferrando, Materials **7** (3), 1830 (2014).
107. F. Shiravand, I. Fraga, P. Cortés, Y. Calventus, and J. M. Hutchinson, J. Therm. Anal. Calorim. **118** (2), 723 (2014).
108. F. Shiravand, J. M. Hutchinson, and Y. Calventus, eXPRESS Polym. Lett. **9** (8), 695 (2015).
109. D. Kong and C. E. Park, Chem. Mater. **15** (2), 419 (2003).
110. J. M. Hutchinson, F. Shiravand, and Y. Calventus, J. Appl. Polym. Sci. **128** (5), 2961 (2013).
111. P. Pustkova, J. M. Hutchinson, F. Román, and S. Montserrat, J. Appl. Polym. Sci. **114** (2), 1040 (2009).
112. J. M. Hutchinson, F. Shiravand, Y. Calventus, X. Fernández-Francos, and X. Ramis, J. Appl. Polym. Sci. **131** (6), 40020 (2014).
113. S. B. Jagtap, V. S. Rao, S. Barman, and D. Ratna, Polymer **63**, 41 (2015).
114. Y. Lu and W. Chen, Chem. Soc. Rev. **41** (19), 3594 (2012).
115. M. Faraji, Y. Yamini, and M. Rezaee, J. Iran. Chem. Soc. **7** (1), 1 (2010).
116. J. P. Wilcoxon and B. L. Abrams, Chem. Soc. Rev. **35** (4), 1162 (2006).
117. A. D. Pomogailo, A. S. Rozenberg, and G. I. Dzhardimalieva, *Metal-Polymer Nanocomposites*, Ed. by L. Nicolais and G. Carotenuto (Wiley, Hoboken, 2005).
118. N. A. Agareva, A. P. Aleksandrov, L. A. Smirnova, and N. M. Bityurin, Perspektiv. Mater, No. **1**, 5 (2009).
119. S. N. Shtykov and T. Yu. Rusanova, Russ. J. Gen. Chem. **78** (12), 2521 (2008).
120. B. A. Rozenberg and R. Tenne, Prog. Polym. Sci. **33** (1), 40 (2008).
121. C. M. Völkle, D. Gebauer, and H. Cölfen, Faraday Discuss. **179**, 59 (2015).
122. S. Yan, Z. Wu, H. Yu, Y. Gong, Y. Tan, R. Du, W. Chen, X. Xing, G. Mo, Z. Chen, Q. Cai, and D. Sun, J. Phys. Chem. **118** (21), 11454.
123. F. Wang, V. N. Richards, S. P. Shields, and W. E. Buhro, Chem. Mater. **26** (1), 5 (2014).
124. M. Wuithschick, B. Paul, R. Bienert, A. Sarfraz, U. Vainio, M. Sztucki, R. Kraehnert, P. Strasser, K. Rademann, F. Emmerling, and J. Polte, Chem. Mater. **25** (24), 4679 (2013).
125. V. N. Richards, N. P. Rath, and W. E. Buhro, Chem. Mater. **22** (11), 3556 (2010).
126. V. I. Irzhak, Rev. J. Chem. **6** (4), 370 (2016).
127. M. Bardaji, P. Uznanski, C. Amiens, B. Chaudret, and A. Laguna, Chem. Commun., No. 6, 598 (2002).
128. M. Nakamoto, Y. Kashiwagi, and M. Yamamoto, Inorg. Chim. Acta **358** (14), 4229 (2005).
129. L. L. Gur'eva, L. I. Kuzub, A. A. Grishchuk, G. A. Estrina, and Ya. I. Estrin, in *Proceedings of XI International Conference on Chemistry and Physicochemistry of Oligomers "Oligomery-2013," Chermogolovka, Russia, 2013* (IPKhF RAN, Chernogolovka, 2013), Vol. 2, p. 127 [in Russian].
130. A. I. Tkachuk, L. I. Kuzub, G. A. Estrina, E. I. Knerel'man, I. I. Khodos, and B. A. Rozenberg, Polym. Sci., Ser. B **55** (3–4), 139 (2013).
131. L. I. Kuzub, L. L. Gur'eva, A. A. Grishchuk, G. A. Estrina, Ya. I. Estrin, and E. R. Badamshina, Polym. Sci., Ser. B **57** (6), 608 (2015).
132. M. Bardaji, P. Uznanski, C. Amiens, B. Chaudret, and A. Laguna, Chem. Commun., No. 6, 598 (2002).
133. M. Nakamoto, Y. Kashiwagi, and M. Yamamoto, Inorg. Chim. Acta **358** (14), 4229 (2005).
134. S. Charan, N. Singh, P. K. Khanna, and K. R. Patil, J. Nanosci. Nanotechnol. **6** (7), 2095 (2006).
135. M. Yamamoto and M. Nakamoto, J. Mater. Chem. **13** (9), 2064 (2003).
136. Y. Kashiwagi, M. Yamamoto, and M. Nakamoto, J. Colloid Interface Sci. **300** (1), 169 (2006).
137. M. Yamamoto, Y. Kashiwagi, and M. Nakamoto, Langmuir **22** (20), 8581 (2006).
138. P. K. Khanna, D. Kulkarni, and R. K. Beri, J. Nanopart. Res **10** (6), 1059 (2008).
139. D. R. Clary and G. Mills, J. Phys. Chem. C **115** (30), 14656 (2011).
140. D. R. Clary, M. Nabil, M. M. Sedeh, Y. El-Hasadi, and G. Mills, J. Phys. Chem. C **116** (16), 9243 (2012).
141. L. I. Kuzub, L. M. Bogdanova, T. S. Kurkin, V. I. Torbov, L. L. Gur'eva, B. A. Rozenberg, and P. V. Buzin, in *Proceeding of Articles "Structure and Dynamics of Molecular Systems," Yal'chik, Russia 2009* (MarGTU, Ioshkar-Ola; Ufa; Moskva; Kazan, 2009), Part 2, No. 16, p. 134.
142. L. I. Kuzub, L. M. Bogdanova, T. S. Kurkin, and P. V. Buzin, in *Proceeding of Articles "Structure and*

Dynamics of Molecular Systems", Yal'chik, Russia 2010 (MarGTU, Ioshkar-Ola; Ufa; Moskva; Kazan, 2010), Part 1, No. 17, p. 340.

143. M. E. Solov'ev, T. F. Irzhak, and V. I. Irzhak, Russ. J. Phys. Chem. A **89** (3), 1642 (2015).
144. M. Sangermano, Y. Yagci, and G. Rizza, Macromolecules **40** (25), 8827 (2007).
145. L. Vescovo, M. Sangermano, R. Scarazzin, G. Kortaberria, and J. Mondragen, Macromol. Chem. Phys. **211** (17), 1933 (2010).
146. G. Kortaberria, P. Arruti, I. Modragon, L. Vescovo, and M. Sangermano, J. Appl. Polym. Sci. **120** (4), 2361 (2011).
147. Y. Yagci, O. Sahin, T. Ozturk, S. Marchi, S. Grassini, and M. Sangermano, React. Funct. Polym. **71** (7), 857 (2011).
148. Y. Yagci, M. Sangermano, and G. Rizza, Polymer **49** (24), 5195 (2008).
149. Y. Yagci, M. Sangermano, and G. Rizza, Macromolecules **41** (20), 7268 (2008).
150. J. Lu, K. S. Moon, and C. P. Wong, J. Mater. Chem. **18** (40), 4821 (2008).
151. J. Lu, K. S. Moon, and C. P. Wong, in *Proceedings of 56 Electronic Components and Technology Conference, San Diego, Piscataway, USA, 2006* (San Diego, Piscataway, USA, 2006), p. 184.
152. H. Gao, L. Liu, Y. Luo, and D. Jia, Mater. Lett. **65** (23–24), 3529 (2011).
153. L. Bogdanova, L. Kuzub, E. Dzhavadjan, E. Rabenok, G. Novikov, and A. Pomogailo, Macromol. Symp. **317–318,** 117 (2012).
154. L. M. Bogdanova, L. I. Kuzub, E. A. Dzhavadyan, V. I. Torbov, N. N. Dremova, and A. D. Pomogailo, Polym. Sci., Ser. A **56** (3), 304 (2014).
155. L. M. Bogdanova, L. I. Kuzub, M. G. Spirin, G. I. Dzhardimalieva, and V. I. Irzhak, Vest. KGTU **18** (16), 10 (2015).
156. T. D. Downing, R. Kumar, W. M. Cross, L. Kjerengtroen, and J. J. Kellar, J. Adhes. Sci. Technol. **14** (14), 1801 (2000).
157. J.-K. Kim and A. Hodzic, J. Adhes. **79** (4), 383 (2003).
158. Y. Gu, M. Li, J. Wang, and Z. Zhang, Carbon **48** (11), 3229 (2010).
159. F. R. Jones, J. Adhes. Sci. Technol. **24** (1), 171 (2010).
160. A. M. Diez-Pascual, M. A. Gómez-Fatou, F. Ania, and A. Flores, J. Phys. Chem. C **116** (45), 24193 (2012).
161. Q. Wu, M. Li, Y. Gu, Y. Li, and Z. Zhang, Composites, Part A **56**, 143 (2014).
162. A. M. Diez-Pascual, M. A. Gómez-Fatou, F. Ania, and A. Flores, Prog. Mater. Sci. **67**, 1 (2015).
163. Y.-L. Zhao and J. F. Stoddart, Acc. Chem. Res. **42** (8), 1161 (2009).
164. M. Terrones, O. Martin, M. González, J. Pozuelo, B. Serrano, J. C. Cabanelas, S. M. Vega-Díaz, and J. Baselga, Adv. Mater. **23** (44), 5302 (2011).
165. M. Aufray and A. A. Roche, Appl. Surf. Sci. **254** (7), 1936 (2008).
166. B. D. Summ and N. I. Ivanova, Russ. Chem. Rev. **69** (11), 911 (2000).
167. V. Georgakilas, M. Otyepka, A. B. Bourlinos, V. Chandra, N. Kim, K. C. Kemp, P. Hobza, R. Zboril, and K. S. Kim, Chem. Rev. **112** (11), 6156 (2012).
168. L. Kong, A. Enders, T. S. Rahman, and P. A. Dowben, J. Phys.: Condens. Matter **26** (44), 443001 (2014).
169. P. Yuan, D. Tan, and F. Annabi-Bergaya, Appl. Clay Sci. **112–113**, 75 (2015).
170. Y. Lvov and E. Abdullayev, Prog. Polym. Sci **38** (10–11), 1690 (2013).
171. D. Mercier, J. C. Rouchaud, and M. G. Barthès-Labrousse, Appl. Surf. Sci. **254** (20), 6495 (2008).
172. M. Aufray and A. A. Roche, Int. J. Adhes. Adhes. **27** (5), 387 (2007).
173. B. J. Henz, T. Hawa, and M. R. Zachariah, Langmuir **24** (3), 773 (2008).
174. A. Jiménez, A. Sarsa, M. Blázquez, and T. Pineda, J. Phys. Chem. **114** (49), 21309 (2010).
175. M. J. Hostetler, J. E. Wingate, C.-J. Zhong, J. E. Harris, R. W. Vachet, M. R. Clark, J. D. Londono, S. J. Green, J. J. Stokes, G. D. Wignall, G. L. Glish, M. D. Porter, N. D. Evans, and R. W. Murray, Langmuir **14** (1), 17 (1998).
176. M. Seong and D. S. Kim, J. Appl. Polym. Sci. **132** (28), 42269 (2015).
177. G. Liu, D. Lv, X. Dong, J. Wu, and D. Wang, J. Appl. Polym. Sci. **133** (13), 43249 (2016).
178. N. G. Sahoo, H. K. F. Cheng, L. Li, S. H. Chan, Z. Judeh, and J. Zhao, Adv. Funct. Mater. **19** (24), 3962 (2009).
179. A. Allaoui and N.-E. El Bounia, eXPRESS Polym. Lett. **3** (9), 588 (2009).
180. K. W. Putz, M. J. Palmeri, R. B. Cohn, R. Andrews, and L. C. Brinson, Macromolecules **41** (18), 6752 (2008).
181. M. L. Auad, M. A. Mosiewicki, C. Uzunpinar, and R. J. J. Williams, Polym. Eng. Sci. **50** (1), 183 (2010).
182. S. Wang, R. Liang, B. Wang, and C. Zhang, Polym. Compos. **30** (8), 1050 (2009).
183. A. H. Barber, S. R. Cohen, S. Kenig, and H. D. Wagner, Compos. Sci. Technol. **64** (15), 2283 (2004).
184. N. Luhyna and F. Inam, in *Proceedings of 2nd International Conference on Advanced Composite Materials and Technologies for Aerospace Applications, Wrexham, UK, 2012* (Wrexham, UK, 2012).
185. Y. Zhang, Y. Wang, J. Yu, L. Chen, J. Zhu, and Z. Hu, Polymer **55** (19), 4990 (2014).
186. Y.-J. Wan, L.-X. Gong, L.-C. Tang, L.-B. Wu, and J.-X. Jiang, Composites, Part A **64**, 79 (2014).
187. Y.-J. Wan, L.-C. Tang, L.-X. Gong, D. Yan, Y.-B. Li, L.-B. Wu, J.-X. Jiang, and G.-Q. Lai, Carbon **69**, 467 (2014).
188. H. Deng, F. Wu, L. Chen, Z. Xu, L. Liu, C. Yang, W. Mai, and B. Cheng, J. Appl. Polym. Sci. **131** (23), 41164 (2014).
189. Z. Li, R. Wang, R. J. Young, L. Deng, F. Yang, L. Hao, W. Jiao, and W. Liu, Polymer **54** (23), 6437 (2013).

190. A. M. Shanmugharaj, J. H. Yoon, W. J. Yang, and S. H. Ryu, J. Colloid Interface Sci. **401**, 148 (2013).
191. L.-Z. Guan, Y.-J. Wan, L.-X. Gong, D. Yan, L.-C. Tang, L.-B. Wu, J.-X. Jiang, and G.-Q. Lai, J. Mater. Chem. A **2** (36), 15058 (2014).
192. R. Konnola, J. Joji, J. Parameswaranpillai, and K. Joseph, RSC Adv. **5** (76), 61775 (2015).
193. K. D. Ziegel and A. Romanov, J. Appl. Polym. Sci. **17** (4), 1119 (1973).
194. L. Yang, S. L. Phua, J. K. H. Teo, C. L. Toh, S. K. Lau, J. Ma, and X. Lu, ACS Appl. Mater. Interfaces **3** (8), 3026 (2011).
195. J. Liebscher, R. Mrówczynski, H. A. Scheidt, C. Filip, N. D. Hadade, R. Turcu, A. Bende, and S. Beck, Langmuir **29** (33), 10539 (2013).
196. K. Jlassi, S. Chandran, M. A. Poothanari, M. Benna-Zayani, S. Thomas, and M. M. Chehimi, Langmuir **32** (14), 3514 (2016).
197. M. Du, B. Guo, and J. Jia, Polym. Int. **59** (5), 574 (2010).
198. K. Prashantha, M.-F. Lacrampe, and P. Krawczak, Adv. Mater. Manufact. Charact. **3** (1), 11 (2013).
199. J. J. Gooding and S. Ciampi, Chem. Soc. Rev. **40** (5), 2704 (2011).
200. P. Sun, G. Liu, D. Lv, X. Dong, J. Wub, and D. Wang, RSC Adv. **5** (65), 52916 (2015).
201. P. K. Ghorai and S. C. Glotzer, J. Phys. Chem. C **111** (43), 15857 (2007).
202. A. P. Kaushik and P. Clancy, J. Chem. Phys. **136** (11), 114702 (2012).
203. R. M. Christensen, *Mechanics of Composite Materials* (Wiley-Intersci. Publ., New York, 1979).
204. H. Miyagawa and L. T. Drzal, Polymer **45** (18), 5163 (2004).
205. G. S. Zhuang, G. X. Sui, Z. S. Sun, and R. Yang, J. Appl. Polym. Sci. **102** (4), 3664 (2006).
206. J. C. Halpin and J. L. Kardos, Polym. Eng. Sci. **16** (5), 344 (1976).
207. M. Ayatollahi, S. Shadlou, M. Shokrieh, and M. Chitsazzadeh, Polym. Test **30** (5), 548 (2011).
208. L. H. Shao, R. Y. Luo, S. L. Bai, and J. Wang, Compos. Struct **87** (3), 274 (2009).
209. D. Shady and Y. Gowayed, Compos. Sci. Technol. **70** (10), 1476 (2010).
210. M. Omidi, H. D. T. Rokni, A. S. Milani, R. J. Seethaler, and R. Arasteh, Carbon **48** (11), 3218 (2010).
211. A. Martone, G. Faiella, V. Antonucci, M. Giordano, and M. Zarrelli, Compos. Sci. Technol. **71** (8), 1117 (2011).
212. T. H. Hsieh, A. J. Kinloch, A. C. Taylor, and I. A. Kinloch, J. Mater. Sci. **46** (23), 7525 (2011).
213. X. Chen, J. Wang, M. Lin, W. Zhong, T. Feng, X. Chen, J. Chen, and F. Xue, Mater. Sci. Eng., A **492** (1–2), 236 (2008).
214. M. Yoonessi, M. Lebrón-Colón, D. Scheiman, and M. A. Meador, ACS Appl. Mater. Interfaces **6** (19), 16621 (2014).
215. P. C. Ma, S. Y. Mo, B. Z. Tang, and J. K. Kim, Carbon **48** (6), 1824 (2010).
216. N. Lachman and H. D. Wagner, Composites, Part A **41** (9), 1093 (2010).
217. C. Corcione and F. Freuli, Polym. Eng. Sci. **53** (3), 531 (2013).
218. X. Wang, J. Jin, and M. Song, Carbon **65**, 324 (2013).
219. M. A. Rafiee, J. Rafiee, Z. Wang, H. Song, Z.-Z. Yu, and N. Koratkar, ASC Nano **3** (12), 3884 (2009).
220. M. Martin-Gallego, M. M. Bernal, M. Hernandez, R. Verdejo, and M. A. Lopez- Manchado, Eur. Polym. J **49** (6), 1347 (2013).
221. X. Sun, H. Sun, H. Li, and H. Peng, Adv. Mater. **25** (37), 5153 (2013).
222. X. Tang, Y. Zhou, and M. Peng, ACS Appl. Mater. Interfaces **8** (3), 1854 (2015).
223. F. Wang, L. T. Drzal, Y. Qin, and Z. Huang, High Perform. Polym. **28** (5), 525 (2016).
224. K. Krishnamoorthy, M. Veerapandian, K. Yun, and S.-J. Kim, Carbon **53**, 38 (2013).
225. J. A. King, D. R. Klimek, I. Miskioglu, and G. M. Odegard, J. Compos. Mater. **49** (6), 659 (2015).
226. Y. Ni, L. Chen, K. Teng, J. Shi, X. Qian, Z. Xu, X. Tian, C. Hu, and M. Ma, ACS Appl. Mater. Interfaces **7** (21), 11583 (2015).
227. K. Kusmono, M. W. Wildan, and Z. A. Mohd Ishak, Int. J. Polym. Sci. **2013**, ID690675 (2013).
228. M. Wang, X. Fan, W. Thitsartarn, and C. He, Polymer **58**, 43 (2015).
229. Q. M. Jia, M. Zheng, C. Z. Xu, and H. X. Chen, Polym. Adv. Technol. **17** (3), 168 (2006).
230. Z. Jiang, H. Zhang, Z. Zhang, H. Murayama, and K. Okamoto, Composites, Part A **39** (11), 1762 (2008).
231. M. Rafiee, F. Yavari, J. Rafiee, and N. Koratkar, J. Nanopart. Res. **13** (2), 733 (2011).
232. V. V. Zuev, Polym. Eng. Sci. **52** (12), 2518 (2012).
233. D. V. Pikhurov and V. V. Zuev, Nanosyst.: Phys., Chem., Math. **4** (6), 834 (2013).
234. A. A. Javidparvar, B. Ramezanzadeh, and E. Ghasemi, Prog. Org. Coat. **90**, 10 (2016).
235. T. Sun, H. Fan, Z. Wang, X. Liu, and Z. Wu, Mater. Des. **87**, 10 (2015).
236. I. A. Al-Ajaj, M. M. Abd, and H. I. Jaffer, Int. J. Min., Metall., Mech. Eng. **1** (2), 93 (2013).
237. G. Stauffer, *Introduction to Percolation Theory* (Taylor and Francis, London, 1985).
238. Yu. Yu. Tarasevich, *Percolation: Theory, Application, Algorithm: Work Book* (Editorial URSS, Moscow, 2002) [in Russian].
239. J. Li, P. C. Ma, W. S. Chow, C. K. To, B. Z. Tang, and J.-K. Kim, Adv. Funct. Mater. **17** (16), 3207 (2007).
240. L. Guadagno, B. De Vivo, A. Di Bartolomeo, P. Lamberti, A. Sorrentino, V. Tucci, L. Vertuccio, and V. Vittoria, Carbon **49** (6), 1919 (2011).
241. L. Liu, K. C. Etika, K.-S. Liao, L. A. Hess, D. E. Bergbreiter, and J. C. Grunlan, Macromol. Rapid Commun. **30** (8), 627 (2009).
242. V. Singh, D. Joung, L. Zhai, S. Das, S. I. Khondaker, and S. Seal, Prog. Mater. Sci. **56** (8), 1178 (2011).
243. J.-E. An and Y. G. Jeong, Eur. Polym. J. **49** (6), 1322 (2013).

244. A. Vavouliotis, E. Fiamegou, P. Karapappas, G. C. Psarras, and V. Kostopoulos, Polym. Compos. **31** (11), 1874 (2010).

245. G. D. Seidel and D. C. Lagoudas, J. Compos. Mater. **43** (9), 917 (2009).

246. P. R. Thakre, Y. Bisrat, and D. C. Lagoudas, J. Appl. Polym. Sci. **116** (1), 191 (2010).

247. S. M. Yuen, C. M. Ma, H. H. Wu, H. C. Kuan, W. J. Chen, S. H. Liao, C. W. Hsu, and H. L. Wu, J. Appl. Polym. Sci. **103** (2), 1272 (2007).

248. B. Tsonos, A. Kanapitsas, G. C. Psarras, and Th. Speliotis, Sci. Adv. Mater. **7** (3), 588 (2015).

249. J. C. Martinez-Garcia, S. J. Rzoska, A. Drozd-Rzoska, S. Starzonek, and J. C. Mauro, Sci. Rep. **5**, 8314 (2015).

250. G. N. Mathioudakis, A. C. Patsidis, and G. C. Psarras, J. Therm. Anal. Calorim **116** (1), 27 (2014).

251. A. Patsidis and G. C. Psarras, eXPRESS Polym. Lett. **2** (10), 718 (2008).

252. S. Singha and M. J. Thomas, IEEE Trans. Dielectr. Electr. Insul. **15** (1), 12 (2008).

253. S. Singha and M. J. Thomas, IEEE Trans. Dielectr. Electr. Insul. **16** (2), 531 (2009).

254. Q. Wang and G. Chen, IEEE Trans. Dielectr. Electr. Insul. **21** (4), 1809 (2014).

255. X. Huang, L. Xie, K. Yang, C. Wu, P. Jiang, S. Li, S. Wu, K. Tatsumi, and T. Tanaka, IEEE Trans. Dielectr. Electr. Insul. **21** (2), 467 (2014).

256. P. Gonon and A. Boudefel, J. Appl. Phys. **99** (2), 024308 (2006).

257. C. Chiteme and D. S. McLachlan, Phys. Rev. B **67** (2), 024206 (2003).

258. S. Nam, H. W. Cho, T. Kim, D. Kim, B. J. Sung, S. Lim, and H. Kim, Appl. Phys. Lett. **99** (4), 043104 (2011).

259. H. W. Cho, S. Nam, S. Lim, D. Kim, H. Kim, and B. J. Sung, J. Appl. Phys. **115** (15), 154307 (2014).

260. H. Gu, S. Tadakamalla, Y. Huang, H. A. Colorado, Z. Luo, N. Haldolaarachchige, D. P. Young, S. Wei, and Z. Guo, ACS Appl. Mater. Interfaces **4** (10), 5613 (2012).

261. J. Huang, Y. Cao, X. Zhang, Y. Li, J. Guo, S. Wei, X. Peng, T. D. Shen, and Z. Guo, AIP Adv. **5** (9), 097183 (2015).

262. K. R. O' Neal, T. V. Brinzari, J. B. Wright, C. Ma, S. Giri, J. A. Schlueter, Q. Wang, P. Jena, Z. Liu, and J. L. Musfeldt, Sci. Rep. **4**, 6054 (2014).

263. A. Kanapitsas, C. Tsonos, G. C. Psarras, and S. Kripotou, eXPRESS Polym. Lett. **10** (3), 227 (2016).

264. X. Zhang, O. Alloul, Q. He, J. Zhu, M. J. Verde, Y. Li, S. Wei, and Z. Guo, Polymer **54** (14), 3594 (2013).

265. S. Wei, Q. Wang, J. Zhu, L. Sun, H. Lin, and Z. Guo, Nanoscale **3** (11), 4474 (2011).

266. J. Zhu, S. Wei, J. Ryu, L. Sun, Z. Luo, and Z. Guo, ACS Appl. Mater. Interfaces **2** (7), 2100 (2010).

267. X. Zhang, O. Alloul, J. Zhu, Q. He, Z. Luo, H. A. Colorado, N. Haldolaarachchige, D. P. Young, T. Shen, and S. Wei, RSC Adv. **3** (24), 9453 (2013).

268. S. H. Song, K. H. Park, B. H. Kim, Y. W. Choi, G. H. Jun, D. J. Lee, B.-S. Kong, K.-W. Paik, and S. Jeo, Adv. Mater. **25** (5), 732 (2013).

269. P. Bonnet, D. Sireude, B. Garnier, and O. Chauvet, Appl. Phys. Lett. **91** (20), 201910 (2007).

270. C. Corcione, F. Freuli, and A. Maffezzoli, Polym. Eng. Sci. **53** (5), 531 (2013).

271. C.-C. Teng, C.-C. M. Ma, C.-H. Lu, S.-Y. Yang, S.-H. Lee, M.-C. Hsiao, M.-Y. Yen, K.-C. Chiou, and T.-M. Lee, Carbon **49** (15), 5107 (2011).

272. C.-W. Nan, G. Liu, Y. Lin, and M. Li, Appl. Phys. Lett. **85** (16), 3549 (2004).

273. S. Yu, S. Yang, and M. Cho, J. Appl. Phys. **110** (12), 124302 (2011).

274. G. Zhang, Y. Xia, H. Wang, Y. Tao, G. Tao, S. Tu, and H. Wu, J. Compos. Mater. **44** (8), 963 (2010).

275. K. Pashayi, H. R. Fard, F. Lai, S. Iruvanti, J. Plawsky, and T. Borca-Tasciuc, J. Appl. Phys. **111** (10), 104310 (2012).

276. V. Sambhy, M. M. MacBride, B. R. Peterson, and A. Sen, J. Am. Chem. Soc. **128** (30), 9798 (2006).

277. S. M. Santhosh and N. Kandasamy, Coatings **5** (2), 95 (2015).

278. X. J. Shen, X. Q. Pei, S. Y. Fu, and K. Friedrich, Polymer **54** (3), 1234 (2013).

279. K. S. Thind, J. Singh, J. S. Saini, and H. Bhunia, Ind. J. Eng. Mater. Sci. **22** (4), 421 (2015).

280. Y. Fu, J. Michopoulos, and J.-H. Song, Comput. Mater. Sci. **107**, 24 (2015).

Translated by T. Soboleva